

UCSF

UC San Francisco Electronic Theses and Dissertations

Title

Rapid Synthesis of 3D Tissues by Chemically Programmed Assembly

Permalink

<https://escholarship.org/uc/item/8j8889s0>

Author

Todhunter, Michael

Publication Date

2015

Peer reviewed|Thesis/dissertation

Rapid Synthesis of 3D Tissues by Chemically Programmed Assembly

by

Michael Todhunter

DISSERTATION

Submitted in partial satisfaction of the requirements for the degree of

DOCTOR OF PHILOSOPHY

in

Biochemistry and Molecular Biology

in the

GRADUATE DIVISION

of the

UNIVERSITY OF CALIFORNIA, SAN FRANCISCO

Copyright 2015

by

Michael Todhunter

ACKNOWLEDGEMENTS

I have had an exceptional opportunity to perform meaningful research at UC San Francisco. I have been equipped with the right resources, surrounded by the right people, and aimed at the right tasks required to pierce the veil. Professor Zev Gartner has provided this environment, in addition to his personal assets of character, insight, and enthusiasm. It has been a pleasure to strive alongside the other members of the Gartner lab. You have provided a work environment from which I could not ask more. In particular, I thank Noel Jee, with whom I have worked closely for a large part of my thesis work, who has pioneered chemically programmed assembly alongside me, and who has contributed a significant portion of the data in Chapter 3. I would also like to thank Justin Farlow, whose mind echoes through the pages of this thesis.

I thank my parents Mark and Sue Todhunter, my dear friends, my cohort of Tetrad 2008, and the community at CoD. Life would not nearly be worth living without you.

I thank Professors Wallace Marshall and Orion Weiner for their advice and expertise steering this project. Professors Jack Taunton, Kevan Shokat, Pam England, and Tejal Desai kindly shared facilities and equipment required for this research. In addition, the UCSF Center for Advanced Technology provided a suite of cutting-edge technology that facilitated this work, and I'd like to specifically thank its Directors Clement Chu and Eric Chow.

I thank my collaborators who have offered varied and valuable perspectives on directions to take this technology. In particular, I thank Sonny Hsiao, Sisi Chen, Yun Suk Na, and Professor David Schaffer. Bijan Boldajipour, Miranda Broz, Audrey Gerard, and Professor Max Krummel. Paolo

Iuliano and Professor Paul Brakeman. Amanda Boggs and Professor Stuart Martin. Finally, Grayson Kochi and Professor Leor Weinberger.

I am grateful to the support staff who have made my various endeavors possible. In particular, I thank Brian Mertz and Matthew Denny for continuously going above and beyond the call of duty when providing logistics. I thank the Tetrad administrators for their continued patience and assistance. There are a great number of people acting invisibly to me who enable smooth day-to-day operations at UC San Francisco. I do not know your names, but your continued work has made mine possible.

I thank Curtis Mosher, who has provided invaluable expertise and support regarding the BioForce Nano eNabler.

I thank the U.S. Department of Defense for supporting this research through the Breast Cancer Research Program Award. I thank the U.S. National Institutes of Health for additional funding support.

Certain figures are reproductions of material previously published and is therefore contributed to by the authors listed therein. A portion of Chapter 3-2 is reproduced in part with permission from Selden NS, Todhunter ME, Jee NY, Liu JS, Broaders KE. Chemically Programmed Cell Adhesion with Membrane-Anchored Oligonucleotides. JACS 134, 765-768 (2012). Other portions of the thesis are reproduced in part with permission from Todhunter ME, Jee NY,

Cerchiari, Hughes AJ, Coyle M, Farlow J, Garbe JC, LaBarge MA, Desai TA, Gartner ZJ. Rapid Synthesis of 3D Tissues by Chemically Programmed Assembly. *Nature Methods* (submitted).

Rapid Synthesis of 3D Tissues by Chemically Programmed Assembly

Michael Todhunter

ABSTRACT

In a multicellular organism, tissue structure is a basis of tissue function. The capacity to create functional tissues has scientific and practical benefits, which has fueled the development of methods to build tissues with controlled structure. Existing technologies are myriad but have important shortcomings. I present a new technology that overcomes these limitations, permitting the synthesis of complex yet well-defined tissue. This technology, dubbed Chemically Programmed Assembly (CPA), exploits DNA hybridization in order to synthesize tissues that span centimeters, possess single-cell spatial resolution, contain multiple cell types, have controlled geometry, and are fully embedded in a variety of extracellular matrices. The CPA process entails attaching living cells to a patterned template surface via DNA hybridization, immobilizing these cells within hydrogel, and releasing them from the template to form microtissues implanted within that hydrogel. I use CPA to demonstrate the synthesis of various microtissues and analyze the behavior of cells within these microtissues.

TABLE OF CONTENTS

1	INTRODUCTION	1
2	METHODS	5
2-1	Patterning with microscale direct writing	5
2-2	Surface passivation chemistry.....	10
2-3	Flow cell construction and related concerns.....	16
2-4	Efficiently attaching cells to surfaces.....	22
2-5	Realizing 3D transfer.....	25
2-6	Detailed protocol for CPA.....	27
3	RESULTS	35
3-1	A variety of microtissue structures can be synthesized with CPA.....	35
3-2	Using CPA to observe tethered suspension cells.....	47
3-3	On the behavior of fibroblasts in CPA culture.....	50
3-4	Branching morphogenesis in CPA culture.....	56
4	THE WAY FORWARD	58
4-1	Technical advances to facilitate adoption and reproducibility of CPA.....	58
4-2	Applications worth striving for.....	66
5	REFERENCES	68
6	APPENDICES	72
6-1	DNA sequences.....	72

TABLE OF TABLES

1-1. Comparison of various tissue synthesis techniques.....	1
3-1. Chart of experimental conditions.	46

TABLE OF FIGURES

1-1. Overview of 3D Tissue Synthesis by Chemically Programmed Assembly.	4
2-1. Mathematical description of droplet volume/spot density relationship.....	9
2-2. Calibration grids for multicomponent patterns.....	9
2-3. Passivating silanes.	14
2-4. Using sessile-drop contact angles to compare silanization reactions and different surfaces. 15	
2-5. Failure modes when preparing silanization reactions.....	15
2-6. Means of flow cell production.	21
2-7. Views of toggle clamp assembly.....	21
3-1. Synthesis of mouse mammary tree pattern from whole mount template.	39
3-2. Transfer fidelity.	39
3-3. Showcase of dense, circular, and fractal patterns.	40
3-4. Synthesis of two-component in-register cellular pattern.	41
3-5. Synthesis of three-component in-register cellular pattern.	42
3-6. Micron-level control of cell-cell spacing.....	42
3-7. Polarization of MCF-10As grown in CPA culture.	43
3-8. Synthesis of large-scale endothelial bed.	43
3-9. Layer-by-layer assembly of CPA cell clusters.	44
3-10. Synthesis of microtissues with defined structure along the Z-axis.	45
3-11. Culture-dependent shape change of Caco microtissues.	45
3-12. Synthesis of three-component microtissues containing multiple functional cell types.....	46
3-13. Dynamics of CPA-tethered Jurkat cells.....	49
3-14. Key frames for movies of CPA-tethered cells.....	49

3-15. Fibroblast/epithelial microtissue array.	52
3-16. Time evolution of cultured fibroblast lines.	53
3-17. Gel deformation by patterned fibroblasts.	54
3-18. Interactions between fibroblasts and epithelial cells.	55
3-19. Translocation of spheroids by aligned fibroblasts.	55
3-20. Branching morphogenesis of heterotypic MCF-10A/T tubes.	57
4-1. Scheme for continuous flow apparatus.	64
4-2. Bestiary of 3D transfer distortions.	65
4-3. Components for magnetic lifting.	65

1 INTRODUCTION

The goal of tissue engineering is to create functional living tissue. Aside from the obvious and lofty applications of regenerative medicine, such capacity would enable the systematic study of tissue structure as well as permit the use of engineered microtissues for drug screening and high-throughput analysis. We have much to gain. The fundamental challenge in tissue engineering is to control the arrangement of a collection of living cells and matrix. The arrangement of cells guides the exchange of chemical, electrical, and mechanical information, which in turn guides their collective behaviors as a tissue¹. Thus, many technologies have been developed with the goal of arranging cells. I assert that CPA combines the most powerful aspects of these varied technologies (Table 1-1), providing a technology with capabilities beyond the current state-of-the-art.

	CPA	Microwell Molding	Inkjet/Laser Printing	Lithography or Microcontact Printing of Cell-adhesion Proteins	Dielectrophoresis	Microfluidic Molding	3D Printing by Extrusion
specification of multiple cell types	yes	no	yes	yes	yes	yes	yes
specification of multiple arbitrary cell types	yes	no	yes	no	no	yes	yes
precise (<1µm) positioning of single cells	yes	limited	no	yes	yes	no	no
3D (cells are in/on hydrogel)	yes	yes	yes	no	yes	yes	yes
high viability	yes	yes	no	yes	yes	yes	no
rapid pattern development	yes	no	yes	no	no	no	yes
production of dense tissues	yes	yes	no	no	yes	yes	no
arbitrary patterns	yes	no	yes	yes	no	no	yes

Table 1-1. Comparison of various tissue synthesis techniques.

The functional properties of tissues arise through the interaction of numerous cell types. These interactions occur in a three-dimensional (3D) setting and in the context of specific tissue structures. For example, the capability of the electric organ, found in fish such as *Campylomormyrus*, to discharge electricity is based on the arrangement of electrocytes into parallel plates, surrounded by insulating matrix, and their simultaneous depolarization triggered by coordinating neurons². The capability of the spinneret, found in silkworms such as *Bombyx*, to extrude silk fiber from fibroin hydrogel is based on the tapered geometry of the spinneret lumen

alongside specific changes in the stiffness of that lumen along its length³. The organization of aligned, cylindrical osteons in compact bone serves to increase the load which the tissue can withstand, and the continuous network of canaliculi within these osteons permits the survival and communication of their resident osteocytes⁴. Ascertaining the relationship between the specific structures and behaviors of tissues remains both a major goal of developmental biology and a requirement for regenerative medicine applications. But, tissue structure is difficult to alter *in vivo*, and tissues' inherent complexity precludes their *de novo* synthesis *in vitro*.

The challenges inherent to controlling tissue structure *in vivo* have motivated efforts to create and control different aspects of tissue structure *in vitro*. Cells and cellular processes can be organized on two-dimensional surfaces by high-resolution patterning of adhesive proteins⁵, and under limited circumstances, these cells can be transferred into 3D culture⁶. Dielectrophoretic patterning⁷ and micromolding⁸ have been used to control tissue size and shape.

Deoxyribonucleic acid (DNA)-programmed assembly, low titer lentiviral infection and genetic mosaics have revealed that heterogeneity in growth factor receptor signaling among mammary epithelial cells can trigger a variety of emergent cell behaviors including collective cell motility, apical and basal cell extrusions, and single hypermotile cells^{9,10,11}. 3D printing tissues have had success at building heterogeneous cell-dense tissue¹¹ but have been limited to low spatial resolution. Despite progress in controlling tissue architecture, no method can simultaneously control the arrangement of multiple cell types, at high spatial resolution, with high viability, within fully embedded 3D matrices.

To provide a better means of controlling tissue structure, we envisioned an alternative strategy for the assembly of complex 3D microtissues using bottom-up, multistep, and layer-by-layer chemically programmed assembly (CPA). In this approach, temporary DNA-based cellular adhesions provide the linkages between cellular building blocks (Figure 1-1). Specific adhesive interactions are programmed by modifying different populations of cells^{10,12-16} with reactive or lipid-modified oligonucleotide sequences. Cells bearing complementary DNA sequences rapidly and specifically adhere to one another according to the rules of Watson-Crick base pairing. To spatially template the microtissue, aldehyde-modified glass substrates are patterned with droplets of aqueous DNA at single-cell spatial resolution via microscale direct writing. The substrate is incubated with cells bearing DNA of complementary sequence, and cells are retained at the desired locations via the resultant hybridization between complementary sequences. After each synthetic step, gentle washing removes unbound cells. The microtissue grows into the third dimension by the rapid and layer-by-layer assembly with successive rounds of CPA. Next, the microtissue is immersed in liquid matrix impregnated with DNase. Gelation of this matrix immobilizes the cells while the DNase simultaneously catalyzes the cleavage of the DNA linking the cells to the substrate. This permits the 3D microtissue to be released from the substrate and overlaid with additional matrix. Dozens to thousands of complex microtissues can be patterned within 1 cm² all within a single optical plane and suitable for culture. Here, we describe the implementation of this method as well as survey some of the microtissues thusly made possible.

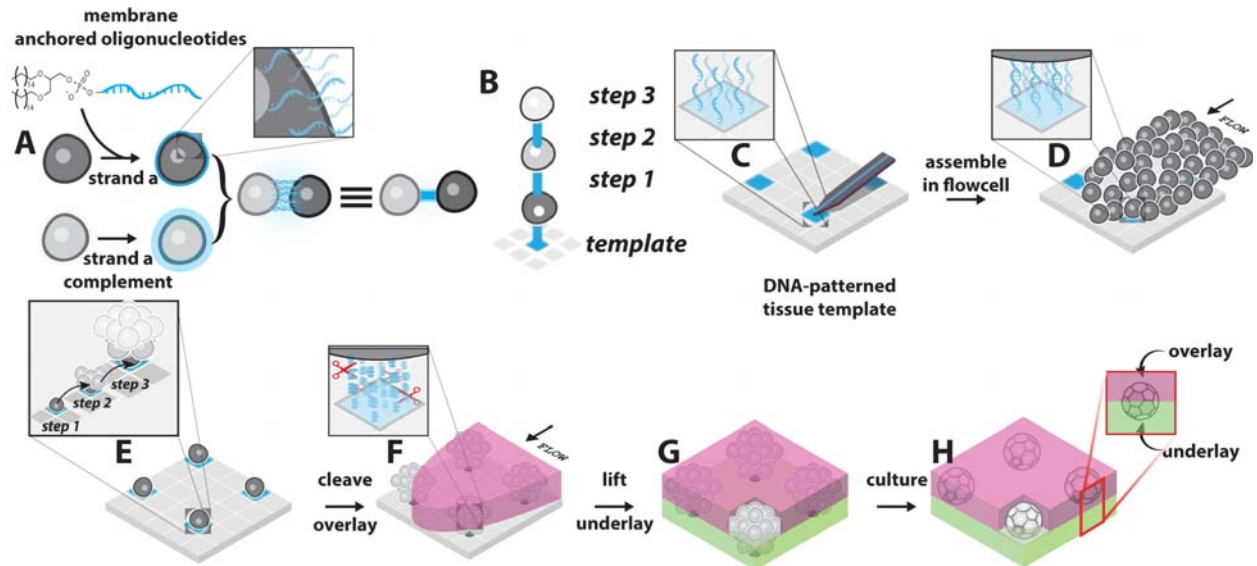


Figure 1-1. Overview of 3D Tissue Synthesis by Chemically Programmed Assembly. Cells are labeled with oligonucleotides (A), and the combination of cell populations labeled with complementary oligonucleotides underlies the principle of bottom-up programmed assembly (B). Oligonucleotides are covalently linked to a glass substrate (C) before cells are flowed across the glass (D). Cells are retained only where DNA hybridization occurs, and iterative flow of complementary cells leads to the assembly of larger structures (E). Flowing DNase-laden matrix over the substrate immobilizes cells while cleaving DNA (F), and the released cells are underlaid with additional matrix (G). Patterned cells grow as microtissues in 3D culture (H).

2 METHODS

2-1 Patterning with microscale direct writing.

To expedite experiments, it is advisable to configure the Nano eNabler for rapid patterning as described in BioForce's Application Note 203¹⁷.

When using microscale direct writing, high concentrations of DNA within a microns-wide droplet yield surprising low densities of DNA conjugated to the patterned surface (Figure 2-1). So, DNA must be spotted at concentrations near the solubility limit. In order to make this possible, I needed to design a spotting solution purpose-formulated for the task of printing high-concentration DNA. At 1x strength, the optimized spotting solution ended up being 22.5 mM sodium citrate, 225 mM sodium chloride, 5% trehalose, 0.1 mg/mL n-octylglucoside, pH 9.5 w/ sodium hydroxide. To formulate this buffer, numerous factors needed to be taken into consideration. First, the buffer needed to be free of amines, thiols, and aldehydes, such that no species would compete with the DNA or the surface in the reductive amination reaction. Notably, the addition of glycerol to the spotting buffer prevented any DNA from being retained on the surface, presumably due to contamination of commercially available glycerol with glyceraldehyde. Second, the buffer needed to contain a surfactant in order for it to suitably wet the Nano eNabler's SPTs, but the surfactant needed to permit well-rounded droplets to form on the surface. Even non-ionic surfactants like Tween-20 and Triton X-100 failed to be suitable for this application, but n-octylglucoside filled the role perfectly. Third, the ionic strength needed to be high enough to prevent rapid evaporation of the DNA droplets but low enough that the buffer would not crash out on the SPT and cause clogs. Fourth, the viscosity needed to be tuned, as this affected the spot size. Fifth, the rates of Schiff base formation and hydrolysis are greatly

influenced by pH, and I empirically determined pH 9.5 to be optimum in terms of the density of DNA ultimately conjugated to the surface. This spotting solution can reliably print down to a relative humidity of about 50% before precipitation occurs.

The library of DNA strands is listed in the appendix. 5'-amine-modified strands are diluted into spotting buffer at a concentration of 2 mM.

DNA is printed onto aldehyde-silanized glass. Our preferred vendor is Schott, and we use specifically their Nexterion AL product. Although it is possible to silanize glass slides at vastly reduced cost relative to the commercial product (using either immersion or chemical vapor deposition), buying slides increases reproducibility and saves time.

The ideal diameter of a DNA droplet, when attempting to anchor a single cell, is three to four microns smaller than the diameter of the cell to be attached. Going beyond this size tends to permit multiple cells attaching to the same DNA spot.

When designing patterns using multiple DNA sequences, I always included a calibration grid in the corner of the pattern. This is a sacrificial pattern component that permits multiple sequences to be aligned with high precision. For patterns with three or more sequences, multiple calibration grids are required (Figure 2-2).

Once patterning is complete, slides are baked at 120° Celsius for 15 minutes, then stored in a vacuum desiccator until use. Patterned slides can be stored for at least a month and possibly much longer.

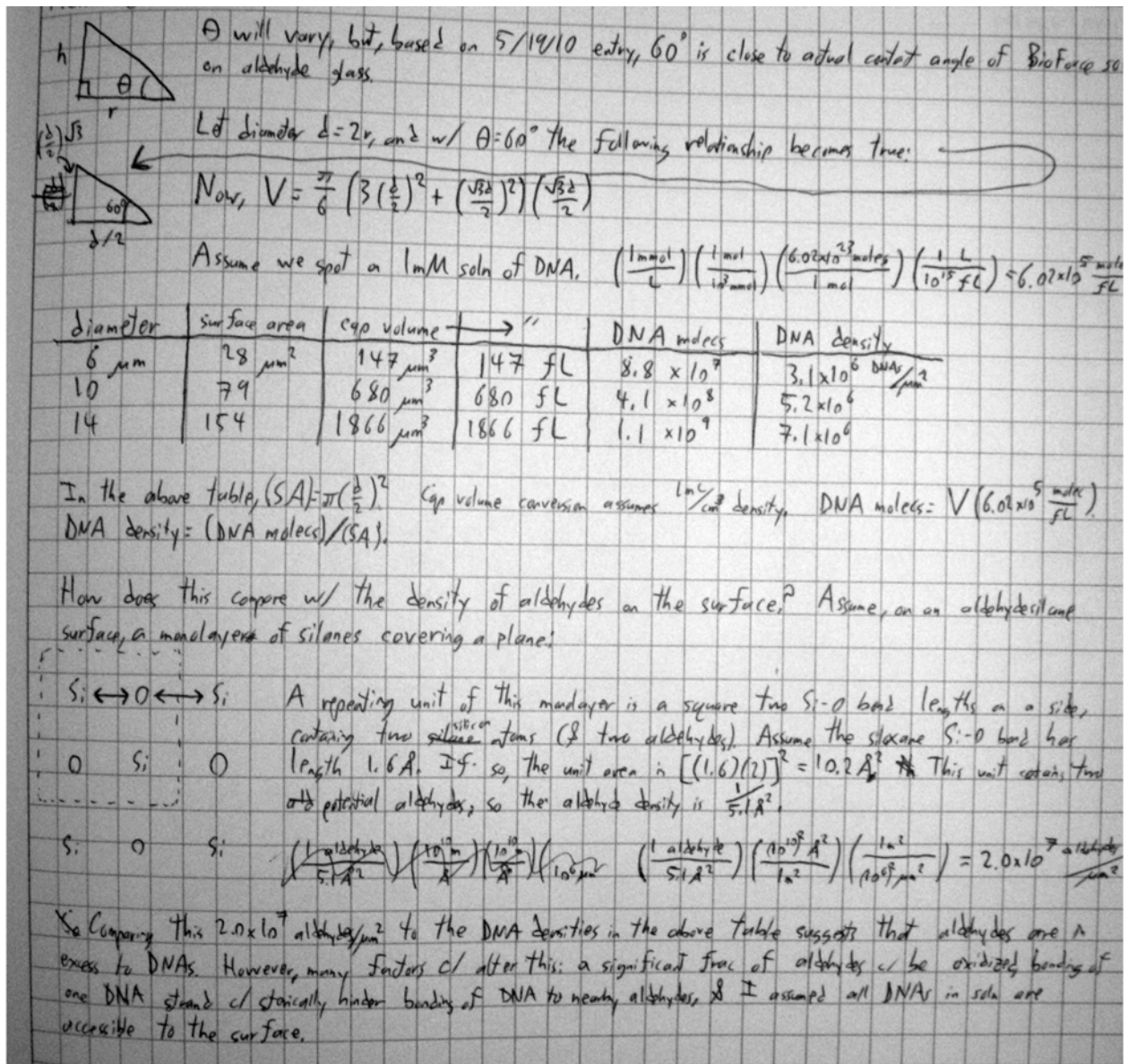


Figure 2-1. Mathematical description of droplet volume/spot density relationship.

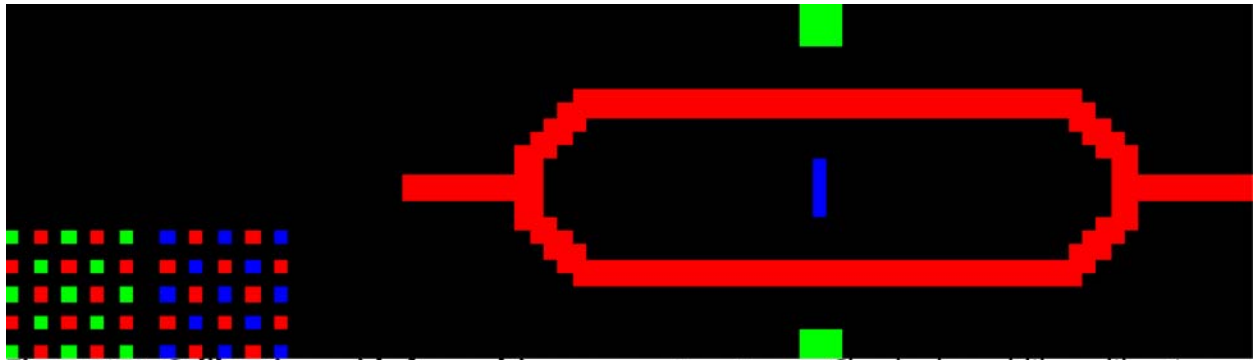


Figure 2-2. Calibration grids for multicomponent patterns. Checkerboard-like calibration grids permit manual alignment of pattern components without sacrificing the relevant portion of the microtissue pattern.

2-2 Surface passivation chemistry.

Successful experiments require cells to adhere specifically to the DNA-patterned glass slide. To an extent, non-specific can be prevented through proper flow buffer formulation (see chapter 2-4), but the primary means of prevention is appropriate surface passivation.

When working with aldehyde-coated surfaces, the first step in passivation is to reduce the surface. For my purposes, the reagent of choice is sodium borohydride, quenching the surface aldehydes by reduction to alcohols while simultaneously reducing the imine-linked DNA into secondary-amine-linked DNA. The progression of surface reduction can be verified by noting the change in contact angle on the glass (Figure 2-4).

A variety of surface passivation methods are available. One approach is to block the surface with a hydrophobic protein such as albumin¹⁸ or casein¹⁹, which will adsorb onto the surface at sites where cells would otherwise be able to stick. Another approach is to coat the surface with a non-fouling polymer - choices include polyethylene glycol²⁰ (PEG), polyhydroxyethylmethacrylate²¹ (polyHEMA), dextrans²², and Pluronics²³. Some of these polymers, especially the PEGs, may produce a brush border on the surface, further preventing adherence of cells. Another approach, which is the one I have adopted, is to render the surface hydrophobic by means of silanization.

Silanization chemistry is a widespread, versatile, and economical means to modify the surface of various substances²⁴. Glass is an excellent substrate for silanization, and there are a variety of silanes available to modify the hydrophobicity of glass.

Throughout my work, I developed two silanization methods for the CPA process. The first method was to use SigmaCote, a hydrophobic silane dissolved in heptane and available from Sigma (Figure 2-3). SigmaCote is a polychlorosilane, meaning that each molecule of silane can react with the surface at multiple distinct sites. Silanes can also react with one another, especially in the presence of water, and hence polychlorosilanes can participate in polymerization reactions. Silane polymerization tends to lead to robust surface modification, but it also means that the reaction never goes to completion - even when the surface is completely silanized, polymerization between silanes can occur indefinitely. This has the potential to produce an interpenetrating network of silane polymers nanometers thick. This is evidenced by the fact that if silanization proceeds long enough, the otherwise transparent glass substrate becomes cloudy. The SigmaCote protocol was to coat the surface with 100 microliters of SigmaCote for 10 seconds, then wash it off with ethanol. This rendered the surface hydrophobic, but there were intermittent side-effects. Sometimes, surfaces treated with SigmaCote would not permit cells to attach. Other times, surfaces treated with SigmaCote would simply not block cell adhesion. These failure modes were persistent, often for weeks at a time, before ceasing of their own accord. The issue with SigmaCote was that there were plausible mechanisms by which trivial environmental factors could drastically change the reaction conditions: environmental humidity could increase silane polymerization, increased airflow could evaporate the heptane and concentrate the reagent, and altering the reaction time by only a few seconds could lead to either over-or-undersilanization. Another potential problem with SigmaCote, and in theory silanes in general, is that the reagent may react with the extracyclic amines on the nitrogenous bases.

The second silanization method that I developed aimed to solve the reproducibility issues associated with SigmaCote. The fundamental difference was to use a monochlorosilane instead of a polychlorosilane. Specifically, I chose tridecafluoro-1,1,2,2-tetrahydrooctyl)dimethylchlorosilane (Figure 2-3), a perfluorosilane. Aside from reaching a higher sessile drop contact angle on glass than SigmaCote, perfluorosilanes should repel both hydrophilic and hydrophobic substances. The drawback to using a monochlorosilane is the reduced reaction rate. To compensate for this, I took several measures to improve the rate of reaction. Adding triethylamine as a catalyst helped (Figure 2-4), as was corroborated by the literature²⁵⁻²⁷. Dipping the surface in acetic acid prior to silanization also helped. I tested several solvents, including heptane, toluene, and dichloromethane. Chlorosilanes must be handled in aprotic solvents to prevent spurious reactions leading to silane polymerization. When working in heptane or toluene, a fibrous precipitate would rapidly form after combination of the triethylamine and silane (Figure 2-5). Unfortunately, when working in dichloromethane, the silane solution needs to be made immediately before use. There are two reasons for this: first, when working in a suitably sized vessel such as a glass Coplin jar, the solvent evaporates on the order of days. Second, on the order of hours, color evolves in the reaction vessel, ranging from straw-colored to red (Figure 2-5). The rate of color formation increases with the freshness of the triethylamine. The hue varies with unknown factors. Preparing a fresh silanization reaction with the appropriate reagents yielded a surface with a sessile drop contact angle in excess of 100° after a 15-minute reaction. I have observed no measurable difference in contact angle upon extending the reaction time to as long as two hours, and I have observed no measurable difference in the extent of cell attachment or background binding. This is highly desirable - it means that the perfluorosilanization reaction, although slow, gives reliable results.

A secondary concern that became apparent while optimizing silanization conditions was that the conformation of DNA on surfaces varied with the hydrophobicity of those surfaces. In my experiments, if the contact angle of a sessile water droplet exceeded approximately 90°, DNA hybridization would become less efficient or cease entirely. Perusing the DNA microarray literature yielded a plausible explanation: on a hydrophilic surface, the native conformation of DNA is to extend into solution, whereas on a hydrophobic surface, the native conformation of DNA is for the nitrogenous bases to be oriented towards the surface, away from solution and therefore inaccessible for hybridization^{28,29}. This is a natural consequence of the amphiphilic character of DNA. To solve this problem, I designed an activation buffer to force the DNA into a conformation favorable to DNA hybridization. This buffer consists of 0.1% Tween-20, 5 mM NaCl, 0.1 mg/mL MgCl₂+CaCl₂, 25 mM acetic acid, pH 2.5, 60° Celsius. The buffer must be prepared fresh, as Tween-20 has a half-life of hours at this pH and temperature, due to ester hydrolysis. The primary effect of this buffer is to protonate the nitrogenous bases, thereby inclining them to be solvated by water. The surfactant and salt are optimized to favor solvation of single-stranded DNA. Once the surface had been exposed to this surface, DNA hybridization can readily proceed for at least a day, as long as the slide is kept submerged in aqueous solution. Waiting for longer periods seems to gradually result in loss of DNA hybridization capacity unless the activation buffer is reapplied. Use of this activation buffer was necessary when dealing with the exceptionally hydrophobic perfluorinated slides, despite the risk posed by such a buffer of acid-mediated depurination³⁰.

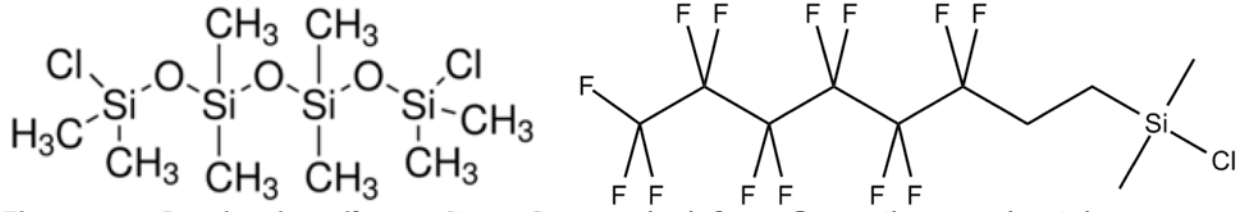


Figure 2-3. Passivating silanes. SigmaCote on the left, perfluorosilane on the right.

+triethylamine



-triethylamine



bare
glass



aldehyde-
coated



alcohol-
coated



perfluoro-
coated

Figure 2-4. Using sessile-drop contact angles to compare silanization reactions and different surfaces. Above, the efficiency of triethylamine towards increasing the extent of silanization is shown by comparing contact angles of water droplets on the silanized glass surface. Below, representative contact angles for a series of different modified glass surfaces are shown.



Figure 2-5. Failure modes when preparing silanization reactions. At left, a cottony precipitate forms when triethylamine and perfluorosilane are mixed in heptane or toluene. At right, color evolves when a reaction vessel is left alone for an hour.

2-3 Flow cell construction and related concerns.

All manipulations of mammalian cells above the patterned surface are done within flow cells. These flow cells are an essential component of the protocol, and there are several reasons for this. First, the flow cell acts as a mold for hydrogel gelation - the depth of matrix in which the microtissues are embedded is a function of the height of the flow cell. Second, the flow cell acts as a handle for the hydrogel during the 3D transfer steps, allowing otherwise impractical manipulation of the paper-thin, fragile hydrogel. Third, the flow cell constrains volume, permitting high cell densities to be reached easily. Finally, the flow cell, of course, permits laminar flow, facilitating mathematically tractable, reproducible wash stringency as well as rapid exchange of buffers across the patterned surface.

Flow cells are cast from polydimethylsiloxane, specifically Sylgard 184. The original molds for the flow cells were simply strips of permanent double-sided tape sandwiched between the bottom of a 15 cm Petri dish and a No. 1.0 coverslip. Coverslips were cut lengthwise into fourths with a diamond scribe, and the tape cut with a razor blade to match, forming 4.5 mm by 18 mm flow channels. PDMS is poured over the flow cells and allowed to cure at 70° Celsius for at least overnight. Due to the tight tolerances on 3M tape and Fisher coverslips, this reliably produces flow channels approximately 200 microns tall.

The principal shortcomings of the tape-and-glass masters are that they are painstaking to fabricate, exhibit variation in their length and width (due to human error when cutting), and begin to fall apart after a dozen or so PDMS casts are made. Figure 2-6 shows such a deteriorated master. As such, I have investigated alternative means of constructing flow cells,

also shown in Figure 2-6. Channels of precise depth can be cut into aluminum blocks, and PDMS poured over this aluminum. Unfortunately, the surface of even highly polished aluminum is not optically smooth and yields flow cells with a matte finish. This is more than just a cosmetic problem, as the flatness of the flow cell ceiling affects the 3D transfer manipulations, with a matte or textured flow cell unable to readily release from the hydrogel during the final steps (see Chapter 2-5 for details). I attempted to smoothen these aluminum-based channels by taking a negative impression in silicone, followed by a positive impression in acrylonitrile butadiene styrene (ABS). ABS is soluble in certain organic solvents, and it is possible to reflow the surface of the mold by partial dissolution in an acetone vapor chamber. Unfortunately, this technique was unable to yield flow cells of sufficient smoothness for 3D transfer manipulations.

I next proceeded to fabricate flow cell molds by 3D printing using the B9Creator photopolymerization printer. This printer could ostensibly produce features with resolution on the order of 25 microns in Z. However, the flow cell molds I fabricated suffered the same smoothness problems. In another attempt to increase smoothness, I took a negative impression of the 3D-printed mold in microcrystalline wax, which has a melting point of around 60° Celsius. Heating the wax to just under the melting point reflows and smoothenes the surface. Next, I took a positive impression in epoxy resin, which is a suitable substrate for casting PDMS flow cells. Unfortunately, the flow cells created in this manner were still of insufficient smoothness, even though they were, at least optically, an improvement over all previous methods.

I next proceeded to replicate the tape-and-glass flow cell molds in epoxy resin. By making a duplicate of a tape-and-glass mold in durable epoxy, I would not solve the issue of length/width variance between flow cells, but I would solve the issue of the molds degrading over time, and one well-crafted tape-and-glass master could be duplicated indefinitely for all CPA users. For this technique, I took a negative impression of the tape-and-glass mold in PDMS (much the same way as I would cast the flow cells themselves), then treated the cured PDMS with SigmaCote. I took a positive impression of the PDMS using epoxy resin and, once cured and itself SigmaCoted, this epoxy became a durable duplicate of the original master. This technique indeed works, and produces flow cells of identical clarity to those of the original master. One drawback to the method is that, due to meniscus effects combined with the softness of epoxy resin, there is a slight dip in the centers of the epoxy masters that leads to non-uniform thickness of the resultant flow cells. I have been able to rectify this problem supporting the back of the epoxy master with a layer of polyurethane resin, which is both firmer than epoxy and also able to fill in the meniscus depression. These epoxy masters are probably the way forward for propagation of CPA. Furthermore, an additional benefit of epoxy is that it can be textured with abrasive tools, permitting alternatives to the wax-based desealing methods described in Chapter 2-5.

For reasons described at length in Chapter 2-5, it is desirable to seal the flow cells by application of physical force using a toggle clamp. This device, consisting of an off-the-shelf clamp screwed into a laser-cut acrylic baseplate, is shown in Figure 2-7. The purpose of the acrylic spacer is to distribute the force of the clamp across multiple flow cells, as well as to fill in the air gap between the roof of the flow cells and the head of the clamp. The purpose of the styrofoam

spacer is to prevent the flow cell from adhering to clamp when declamping occurs. The low contact area between the styrofoam and the PDMS minimizes the possibility of adhesion.

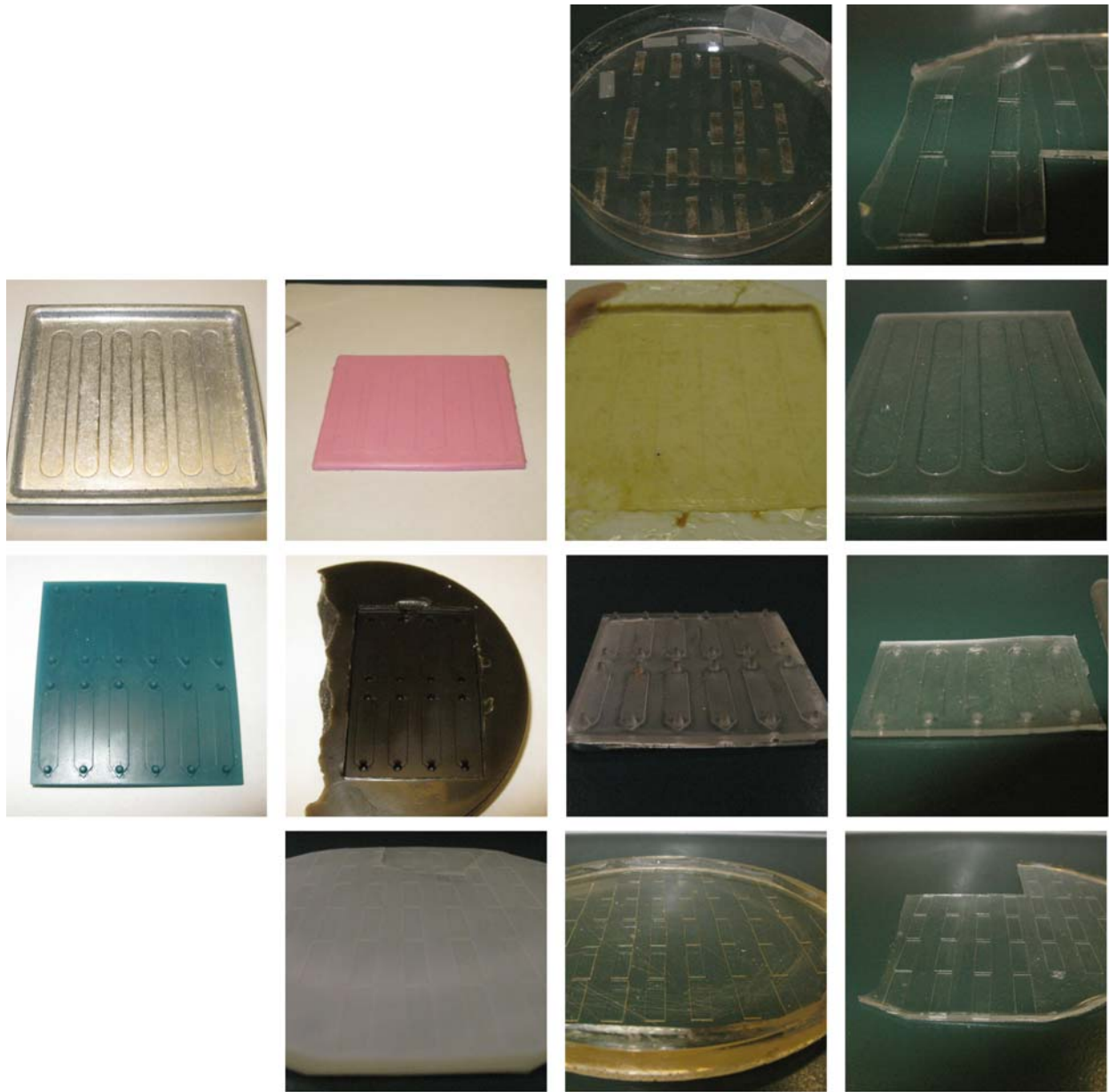
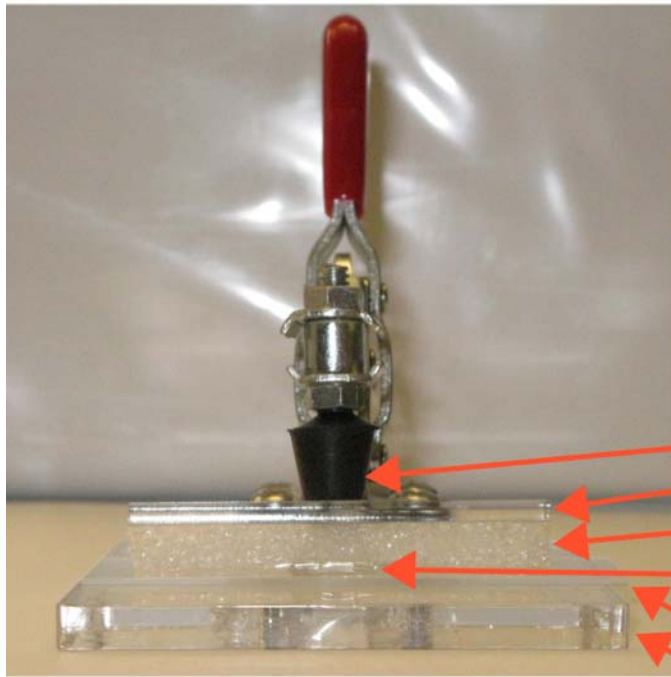
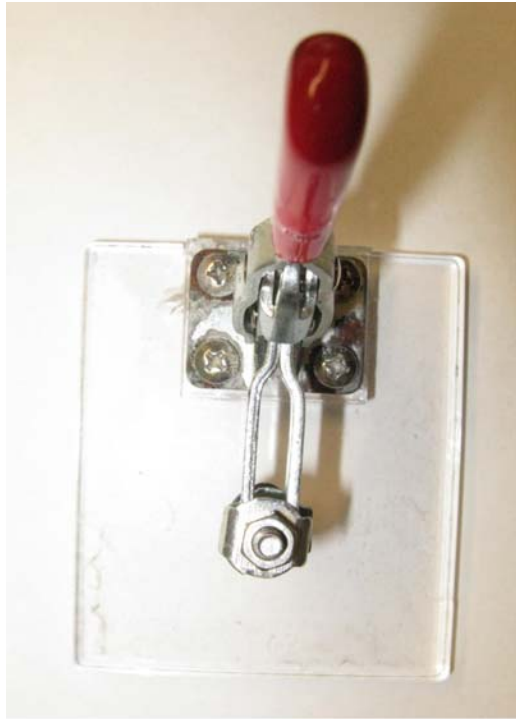


Figure 2-6. Means of flow cell production. Row 1: a damaged tape-and-glass master, with transparent PDMS flow cells at right. Row 2: aluminum, silicone, and ABS flow cell masters, with resultant textured flow cells at right. Row 3: photopolymerized resin, wax, and epoxy flow cell masters, with resultant textured flow cells at right. Row 4: Opaque SigmaCoted PDMS and epoxy dish flow cell masters, with resultant transparent flow cells at right.



- clamp head
- acrylic spacer
- styrofoam spacer
- flow cell
- patterned slide
- baseplate

Figure 2-7. Views of toggle clamp assembly. Above, birds-eye and side views of an unloaded toggle clamp. Below, head-on view of a toggle clamp loaded with flow cell and appropriate spacers.

2-4 Efficiently attaching cells to surfaces.

A major technical consideration when developing this project was how to maximize the quality of the produced patterns. When patterning cells, it is essential that the cells are everywhere that they're supposed to be and nowhere that they're not supposed to be.

How do we get the cells everywhere they're supposed to be? First, the density of DNA on the surface must be maximized, and the appropriate considerations for this are described in Chapter 2-1. Second, the density of DNA on cell surfaces must be maximized. This was outside the scope of my own work, but the Selden and Weber papers included studies of how DNA incorporation varied with factors such as reaction time, temperature, and DNA concentration. Third, the density of cells within the flow cell must be optimized - under most circumstances, the ideal density is, when viewed from above, a monolayer of cells. The ideal density is lower for cell types that exhibit aggregative behaviors. Fourth, the temperature must be minimized. DNA hybridization becomes increasingly favorable as temperature lowers, due to the entropic component of the hybridization free energy. As a side benefit, lower temperatures promote cell viability. As such, the ideal temperature is slightly above the freezing point of the buffer - our current target is 1° C.

A couple of procedural variations have been implemented to further maximize cell attachment. One variant is to have the flow cells centrifuged at slow speed, ~180 g 3 minutes with slow acceleration and deceleration in a swinging bucket centrifuge. This forces the mammalian cells into compliance with the solid surface, increasing the potential contact area between the cells and the glass. Another variant is to gradually push the cells through the flow cell using a "cycling"

procedure, wherein small (3 μL or $\sim 10\%$ of the flow cell volume) amounts of liquid are repeatedly pulsed by pipet. These small volumes are sufficient to impel the motion of the mammalian cells through the flow cell without elevating them into the central streamlines, instead "rolling" along the patterned face. In this manner, the cells can each sample a much greater fraction of the surface than would otherwise be possible.

Minimizing non-specific background is primarily a matter of passivating the surface properly. The perfluorosilanization described in Chapter 2-2 is sufficient to do that. One issue that can produce non-specific background despite silanization is insufficient height of the flow cell. A flow cell cast from a deficient master, or a flow cell overcompressed by a clamp, or a flow cell with an insufficiently thick and therefore buckling ceiling will exhibit difficulty eluting cells regardless of surface passivation. This may be due to decreased flow rates through a flow cell of reduced cross-sectional area.

Manipulations are much improved by resuspension of cells into an appropriate flow buffer. As of this writing, the ideal flow buffer is calcium/magnesium-free PBS supplemented with 0.01% EDTA, 2% BSA, and 0.1% Pluronic F68. The primary consideration in a flow buffer is to prevent cell aggregation, and therefore a rational starting point is the same buffers used in FACS protocols. The Pluronic was added for a separate reason. In multiple experiments, it had been observed that attaching primary mammary fibroblasts to a pattern reduced the efficiency of attachment for subsequent cell types, even to different locations on the pattern. It is unclear why this happens, but one plausible mechanism is deposition of protein, especially matrix protein,

that occludes the surface DNA. Regardless of the mechanism, addition of Pluronic to the flow buffer appears to decrease the magnitude of this effect.

Minimizing cross-hybridization is primarily a matter of good sequence design, described at length in Chapter 2-7. Cross-hybridization becomes increasingly problematic as temperature decreases for the same reason that low temperature is desirable: DNA hybridization, both specific and otherwise, becomes more favorable as temperature drops. Thus, there is a trade-off between attachment efficiency and background. Generally, when cross-hybridization occurs, it can be purged by flowing sufficiently high velocity liquid through the flow cell, usually achieved by tilting the flow cell 90° and forcefully injecting flow buffer at the inlet. In principle, there are a great many factors that affect DNA hybridization, and wash buffers could be designed that vary these factors appropriately.

There is another form of background that appears to be specific to microtissues made with iterated rounds of programmed assembly. When programmed assembly is used to make multiple-cell clusters, it is important to note that these clusters do not possess smooth, continuous surfaces. Therefore, it is possible - even inevitable - that cells under flow can become stuck within the interstices on the surface of existing clusters. It may be possible to dislodge such background by varying the direction of flow during washes, but at the time of this writing, the best way to avoid this issue is to build the cell clusters last when making heterotypic microtissues.

2-5 Realizing 3D transfer.

Theoretically, there are only two requirements to realizing 3D transfer: the DNA linking the cells to the surface must be cut, and the cells must be immobilized in matrix such that the information content of the pattern is not lost. But practically speaking, 3D transfer is the most technically demanding part of the CPA process. In this section, I describe the practical considerations towards successful 3D transfer.

Once the appropriate microtissues have been assembled by CPA, several steps need to proceed in sequence. First, liquid matrix, supplemented with DNase, must be flowed into the flow cell, then allowed to set. Second, the flow cell must be transferred off the patterned slide, releasing the microtissues along with it. Third, the flow cell must be placed onto liquid underlay matrix, which is allowed to set in kind. Fourth, the flow cell must be removed from the matrix, leaving the microtissues fully embedded in gel and freed of both their templating surface as well as their flow cell.

The first step, flowing liquid matrix, has as its principal challenges matrix viscosity and air bubble entrainment. In principle, any matrix that can exist in both liquid and gelled forms without killing cells is compatible with CPA. This includes temperature-gelling matrices like Matrigel, collagen, and agarose. This includes time-gelling matrices like fibrin. This includes photopolymerizing matrices, namely acrylate-conjugated materials such as PEG-acrylate and hyaluronan-acrylate. However, if the viscosity of the liquid matrix is too high, cells will detach from the pattern. At best this results in some microtissues simply being depleted of cells, and at worst this results in displaced cells getting stuck in downstream microtissues. To mitigate this

problem, flow velocity can be reduced. Additionally, the volume of matrix flowed can be minimized - in principle, two flow cell volumes of matrix should be sufficient to replace the majority of liquid within the flow cell. Intuition would suggest that one flow cell volume of matrix should be sufficient to displace the entirety of flow buffer with matrix, but this is incorrect. The parabolic nature of laminar flow means that multiple flow cell volumes must be flowed before the entire internal volume is displaced.

The second step, transfer off the patterned slide, requires the adhesivity between the surface, flow cell, and hydrogel to be within certain tolerances. The surface must be as non-adherent as possible, hence the previously described silanization process. In contrast to typical PDMS flow cells, which are plasma-treated prior to surface bonding, CPA's flow cells use native PDMS, which is hydrophobic. Native PDMS binds only weakly to the silanized glass. To prevent leakage of fluid under the side walls of the flow cell, physical pressure is applied using a toggle clamp, as described in Chapter 2-3. When it comes time to perform 3D transfer, the toggle clamp is released and the physical pressure removed. To even further decrease interactions between flow cell and surface, the contact area between them is reduced. This is typically achieved by coating the bottom of the side walls with a layer of microcrystalline wax, which lends a rough surface.

The third step, placement onto underlay, requires careful manipulation of the hydrogel and flow cell to ensure level, centered placement. The fourth step, flow cell removal, requires minimal adhesion between the flow cell and the hydrogel. This is sufficiently achieved simply by using natively hydrophobic PDMS.

2-6 Detailed protocol for CPA.

MATERIALS & REAGENTS

tridecafluoro-1,1,2,2-tetrahydrooctyl)dimethylchlorosilane (Gelest, SIT8170.0)

triethylamine (Fisher, O4884-100)

dichloromethane (Fisher, AC40692-0040)

absolute ethanol (Fisher, BP2818-4, but UCSF Storehouse might be cheaper)

glacial acetic acid (Fisher, BP1185-500)

sodium borohydride (Fisher, AC41947-1000)

Sylgard 184 (Fisher, NC9644388, but Fisher ships this anomalously slowly. Consider Amazon for faster shipping)

microcrystalline wax (Douglas & Sturgess, SC-1159)

Turbo DNase (Life Technologies, AM2238)

grease pencil (Amazon, Dixon Peel-Off China Marker)

sharp curved tweezers (such as Roboz, RS-4951)

2 mm styrofoam sheet

2 mm acrylic sheet

5'-dialkyl DNA (Gartner lab)

mounted toggle clamp (Gartner lab)

In addition: phosphate-buffered saline calcium/magnesium-free, bovine serum albumin, Tween-20, sodium chloride, calcium chloride, magnesium chloride, distilled water (dH₂O), and Matrigel.

PREPARATION

In advance, prepare Priming Buffer: 0.1% Tween-20, 5 mM NaCl, 0.1 mg/mL MgCl₂+CaCl₂, 25 mM acetic acid, pH 2.5. 60 Celsius. Use same day because Tween-20 degrades within a day under warm acidic conditions due to ester hydrolysis.

In advance, prepare Flow Buffer: 2% BSA in PBS, calcium/magnesium-free. Sterile-filtered, ice-cold.

In advance, cast PDMS flow cells from glass and tape mold.

TREATMENT OF PATTERNED SLIDE AND FLOW CELL ASSEMBLY

Prepare a solution of 0.25% NaBH₄ in 25% ethanol, 75% PBS. 25 mL is more than enough for one slide. Place the slide, in its dish, on a shaker at 120rpm. Add enough NaBH₄ solution to cover, and let it react for 15 minutes. Pipet the NaBH₄ soln and replace it in its vessel.

WARNING: NaBH₄ evolves H₂ gas. Do not tightly cap any containers of this solution, and do not store near an open flame. Do not dump fresh NaBH₄ solutions down the drain. Either inactivate with dilute acid or wait at least 24 hours for the solution to spontaneously decompose.

Make a solution of 0.1% SDS (diluted 1/20 in dH₂O from 2% SDS) and pour enough into the slide's dish to cover the slide. Swish 10 times, dump solution into sink (make sure you're

holding the slide!). Repeat SDS wash. Then, repeat three more times, substituting pure dH₂O for the SDS solution. That makes five washes total.

Fill a Coplin jar with 60 mL dichloromethane. Add 600 µL perfluoro-dimethylchlorosilane (specifically, (tridecafluoro-1,1,2,2-tetrahydrooctyl)dimethylchlorosilane). Add 600 µL triethylamine. Mix. Fill five 50 mL polypropylene conical tubes with: dichloromethane, dichloromethane again, ethanol, water, pH 4.5 25 mM acetic acid in water.

Immerse the slide in 10% acetic acid. Dry slide under stream of air. Immerse slide in Coplin jar of DCM+silane+TEA. Let shake at 120 rpm for 15 minutes. Then, using paddle tweezers, transfer slide into conical tubes of successive washing solutions: 1st DCM-> 2nd DCM-> ethanol -> dH₂O. For each wash, securely cap the conical tube and invert ten times before transferring slide to next tube in the series. Upon transfer to tube of pH 4.5 acetic acid, shake at 120 rpm for 30 minutes. Remove slide from tube and dry under stream of air. WARNING: dichloromethane is not compatible with all plastics. It is advisable to verify, before use, that your conical tubes do not dissolve or soften upon solvent exposure. It is advisable to discard tubes after use.

Using a razor blade, cut out PDMS flow cells. Cut an inlet and outlet from either end. Clean the PDMS by applying Scotch tape to the surface, pressing firmly, and peeling it away. Repeat this twice for both surfaces of the PDMS. Using a wax stick, apply a thin layer of microcrystalline wax to the ceiling of the flow cell. Apply the PDMS, channel-side down (you should be able to feel the channel with your finger as well as see it), to the slide, centering the flow cell over the patterned region. Using the blunt edge of a razor blade, press the PDMS into the slide to

establish a light seal. WARNING: if the slide is on a hard surface (like a benchtop), pressing into the PDMS can fracture the slide. Use a soft surface, such as a self-healing mat (or possibly a mousepad) for this step.

Use a grease pencil to draw barriers between the inlets and outlets of adjacent flow cells. This prevents cross-contamination between adjacent flow cells and prevents any liquid that accumulates at the inlet or outlet from creeping along the sides of the flow cells.

Place the slide on the base of the mounted toggle clamp. Place a styrofoam spacer atop the flow cells. Place an acrylic spacer atop the polystyrene. Clamp down on the acrylic with gentle pressure. The slide should be sufficiently clamped to immobilize it but not so strongly clamped that the flow cells are compressed.

Prime the flow cell with Priming Buffer. Pipet 100-200 μL and slowly inject it into the flow cell, tilting the flow cell vertically such that the flow is against gravity. Try not to introduce air bubbles into the flow cell. Let the flow cell incubate 1-2 minutes before flushing it with another 100-200 μL of warm Priming Buffer. Repeat for three total exchanges of Priming Buffer. Then, equilibrate each flow cell with 300 μL Flow Buffer. Add a small volume (10-30 μL) of Flow Buffer to the inlet and outlet to prevent evaporation from the inside of the flow cell and store, covered, at 4° C, until ready to attach cells. Flow cells can be stored in this manner for up to one day as long as evaporation is prevented.

PREPARATION OF DNA-LABELED CELLS

Prepare a suspension of cells by whatever means is appropriate. For MCF-10As, I rinse adherent cells with PBS+EDTA and trypsinize with 0.05% trypsin for 15-25 minutes.

Take an aliquot of dry lipid-DNA and resuspend into 250 μL PBS CMF to make a 5.5 μM soln. Thoroughly mix, pipetting up/down at least 20 times as well as vortexing for at least 5 seconds. Leftover lipid-DNA should be stored frozen at -20°C and can be used in future experiments, again mixed thoroughly after being thawed.

Spin cells as appropriate for your cell line (for MCF-10As, we spin 4 minutes at 300 g).

Resuspend into PBS CMF and count cells. Transfer 1.5×10^6 cells to an Ep tube and, again, spin. Remove the supernatant, being careful to remove as much supernatant as possible (we use a P200 or P20 micropipet to carefully remove residual supernatant from the pellet). Resuspend cells in 50 μL of 5.5 μM lipid-DNA. Agitate 5-15 minutes (such as on a rocker). Then, add 1 mL PBS CMF. Spin and again resuspend in 1 mL PBS CMF. Spin and finally resuspend into 50 μL Flow Buffer to make a high-concentration solution of 3×10^7 cells/mL.

ATTACHMENT OF DNA-LABELED CELLS TO PATTERNED SLIDE

Inject 20 μL of high-concentration, DNA-labeled cells into each flow cell. Let the cells settle for three minutes at 4°C . Add 3 μL cells to inlet, and "cycle" the flow cell by pipetting 2 μL up at outlet and back down at inlet, moving the cells through the flow cell without dilution. Repeat this cycling ten times. Carefully, slowly, inject 100 μL Flow Buffer into each flow cell. Repeat 2-4

times until flow cells are mostly cleared of cells. Then, wash with 1-3 mL Flow Buffer to remove any remaining cells aberrantly stuck to the surface.

If cell assemblies or multiple cell types are desired, repeat the above paragraph with additional quantities of appropriately labeled cells.

EMBEDDING PATTERNED CELLS INTO MATRIGEL

From this point on, it is recommended to perform all manipulations with the most sterile technique feasible, preferably inside a cell culture hood.

Prepare a solution of ~9 mg/mL Matrigel supplemented with 2% v/v Turbo DNase (2 U/ μ L, Life Technologies). Prepare 200 μ L for each flow cell. Make sure to keep Matrigel on ice at all times and minimize the introduction of air bubbles into the solution. To clear air bubbles, vacuum degas the Matrigel on ice for five minutes.

Place the flow cells onto an ice-cold surface. Using a pre-chilled pipet tip, flow 100 μ L Matrigel+DNase into each flow cell. Matrigel is viscous, and this flow-through will be slow. Tilt the flow cell, even as much as 90 degrees, to assist flow-through. When sucking up molten gel from the outlet, under no circumstances bring the pipet tip closer than 1mm to the edge of the PDMS (doing so can induce sheer forces which, depending on the gel, can depopulate your pattern). Working carefully, declamp the flow cells, being careful to not lift the flow cells from

the surface or introduce air bubbles into the gels. Let Matrigel gel in 37° C incubator for 15 minutes.

For each flow cell, prepare 100 µL of Matrigel diluted 50% with PBS CMF. Working on an ice-cold surface, use an inoculating loop to spread 80 µL diluted Matrigel on a 3.5 cm cell culture dish (an inoculating loop is preferred over alternative methods due to its reduced propensity to scratch the plastic dish). Let the dilute Matrigel find its level within the dish, on ice, for at least 3 minutes. Then, let the Matrigel gel in 37° C incubator at least 15 minutes, until you are ready to continue with subsequent manipulations.

Remove the flow cells from the incubator. Pipet 20 µL culture media around the edges of the flow cell. Using a sterile razor blade, press against the edge of the flow cell and slide the flow cell towards the edge of the slide. Carefully invert the slide, and use the razor blade to push the flow cell off the edge, transferring the flow cell onto the face of the blade. Pipet 30 µL cold Matrigel onto the center of a 3.5 cm dish, pluck the flow cell from the face of the razor blade, and deposit the flow cell onto the cold Matrigel. Leave the dish on the receiving platform for at least 1 minute to allow the flow cell to find its level. Then, let the underlay gel in 37° C incubator for 15 minutes.

Repeat the above paragraph's manipulations for each flow cell, in turn.

Remove the dishes from incubator and add 3 mL prewarmed tissue culture media to each dish, enough to submerge the flow cells. It is best to slowly drip the media directly on top of the

PDMS to thoroughly wet its surface. Otherwise, the hydrophobic nature of the PDMS may prevent its complete immersion. Once the PDMS is immersed, use sharp curved tweezers to slide the PDMS up and off of the gel, exposing it to the media. Pluck the PDMS and discard. The patterned 3D microtissues are now ready for any downstream growth, observation, or manipulation.

3 RESULTS

3-1 A variety of microtissue structures can be synthesized with CPA.

Using the method described in Chapter 2, I have been able to make a variety of microtissues of varied composition. The first part of this chapter consists of a gallery of images representative of the sorts of microtissues that can be made with CPA.

Owing to the capacity of the Nano eNabler to process bitmap images, any pattern which can be rasterized can be rendered as a pattern of DNA droplets and, subsequently, a microtissue.

Figure 3-1 shows a large-scale cellular pattern, nearly 2cm across, based on a whole mount image³¹ of a mouse mammary tree³². Figure 3-2 shows the preservation of this pattern across the 3D transfer process. It is important to note that the details of the pattern present on the patterned 2D surface are retained even after the cells are embedded within soft hydrogel. Figure 3-3 shows a variety of other patterns, each with its own particular features, that can be successfully patterned using the Nano eNabler.

A strength of microscale direct writing is the ease with which multiple patterns can be aligned with one another. For techniques such as photolithography and microcontact printing, while it is possible to print multiple patterns in register, doing so requires sophisticated means to align subsequent patterns, and if a mistake in alignment is made, the pattern is entirely lost. The one-at-a-time nature of direct writing, combined with the Nano eNabler's on-board camera, permits minute adjustments to be made and verified before possibly damaging the pattern. Figure 3-4 demonstrates the symmetrical alignment of a two-component pattern, and figure 3-5 demonstrates precision alignment of a three-component pattern. In principle, as long as an

adequate number of orthogonal DNA strands has been designed, there is no limit to the number of unique patterns that can be aligned to one another within a pattern. Figure 3-6 goes on to show the degree of positional control possible on the Nano eNabler with a two-component pattern of varied spacing. The stage translation motors ostensibly have precision down to 0.1 μm . At this level, what limits the precision of cell position is the variance of the diameters of the cells themselves, rather than the patterning itself. Figure 3-6 additionally demonstrates that the condensation of pairs of neighboring MCF-10A epithelial cells varies with the distance between cell pairs.

In order for a microtissue synthesis strategy to be useful, microtissues need to be viable under prolonged culture. Figure 3-7 demonstrates, by immunofluorescence, that the polarization of nuclei and alpha-6 integrin occurs on the order of approximately a week when MCF-10As are grown from single cell grids via CPA. This demonstrates that the cells are alive, capable of growth, and engage in polarization behaviors well-established by literature. Figure 3-11 shows another cell type, Caco-2 intestinal epithelial cells, grown under week-long culture, with the final appearance of the Caco-based microtissue to be a function not only of the initial cell pattern but also the media conditions throughout the experiment.

A unique property of CPA is the capacity to build up dense and/or complex patterns from relatively simple templates. This build-up approach is demonstrated in figure 3-5, where four successive rounds of CPA bring microtissues from one or two cells up to several dozen. Iterating CPA on single cells produces dome-shaped microtissues, whereas iterating on CPA on more complex patterns can be used to make structures such as endothelial beds, as seen in figure 3-6,

or the aforementioned Caco-2 tubes in figure 3-11. Such structures can be big enough to be visible by eye. The principle limitation to the amount of CPA iteration is the height of the flow cell used. My experience suggests that microtissues exceeding 80 μm tall are unstable within a standard 200 μm flow cell. One straightforward explanation for this limitation is the shear force across the microtissue, which grows linearly across constant distances as the microtissue grows into the central streamlines of the flow cell. Figure 3-12 shows microtissues consisting of multiple components being built up by independent CPA processes - for the MCF-10ATs, shown in green, spheroids are produced, while cords are produced for the HUVECs, in red.

What goes beyond simply building up patterns to occupy greater volume is the capacity to produce patterns containing structural information in both the xy plane and along the z axis. Figure 3-10, top left, demonstrates the capacity to produce a stratified microtissue, with one cell type positioned above the other. Stratification is an interesting motif, common to such tissues as the skin and cerebral cortex. Figure 3-10, top right, demonstrates the capacity to totally enclose a first cell type within a layer of a second cell type. Figure 3-10, middle row, demonstrates this capacity using human mammary epithelial cells, and the synthetic scheme for this process is shown in the bottom row. In principles, other structures such as an overpass of intersecting tubes could also be produced. It is structures such as these, containing occluded internal geometry, which can be produced by no other tissue engineering methods.

The variety of CPA processes used in these figures is summarized in Table 3-1.

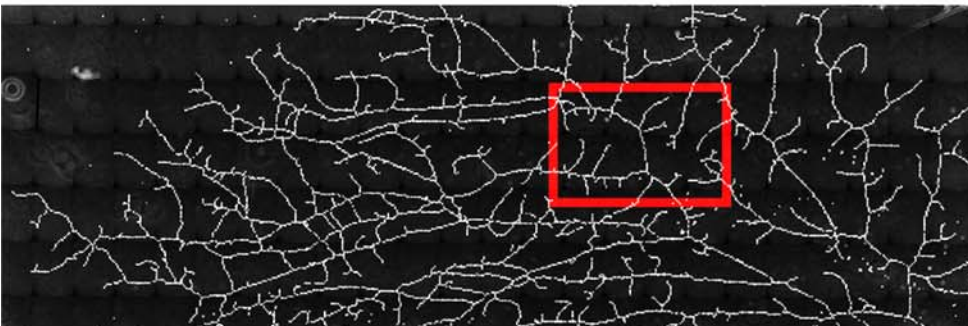
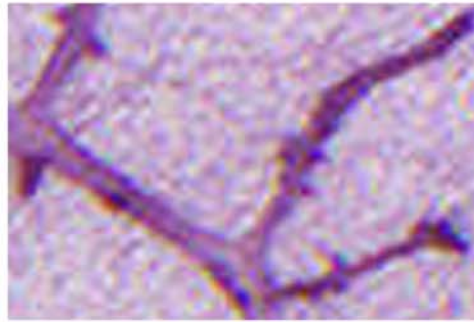
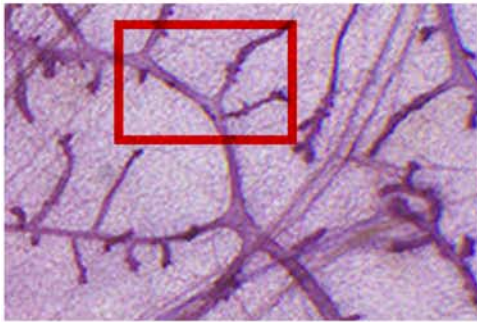
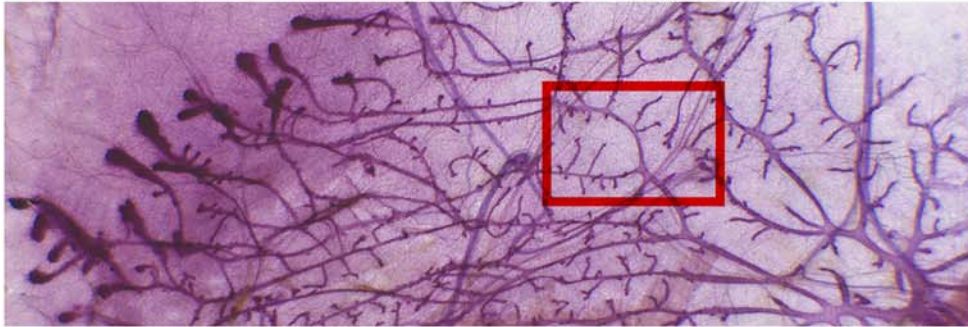
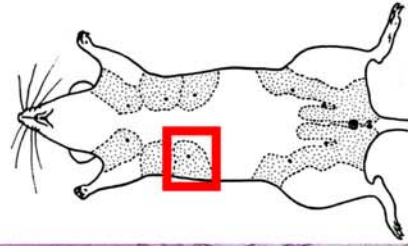


Figure 3-1. Synthesis of mouse mammary tree pattern from whole mount template.

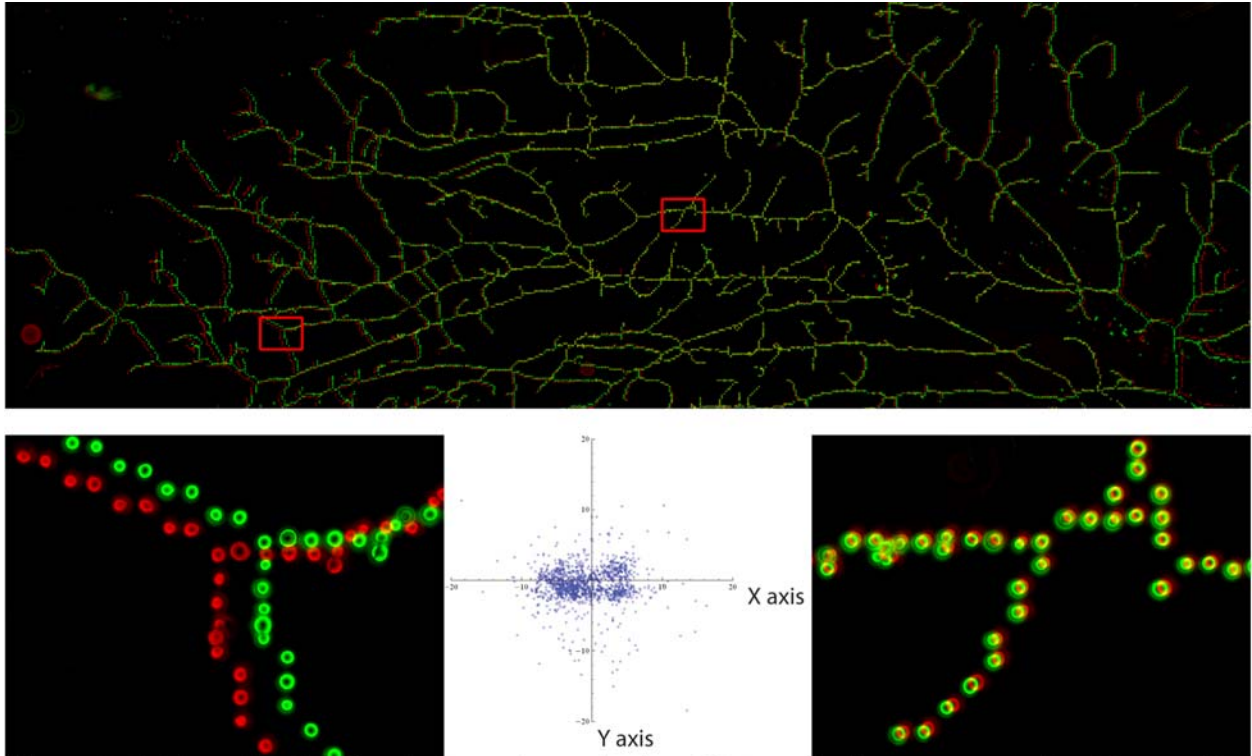


Figure 3-2. Transfer fidelity. Pattern shown before 3D transfer in green and after 3D transfer in red. Selected areas magnified. Scatterplot shows change in position of cells before/after transfer, revealing anisotropy along X axis.

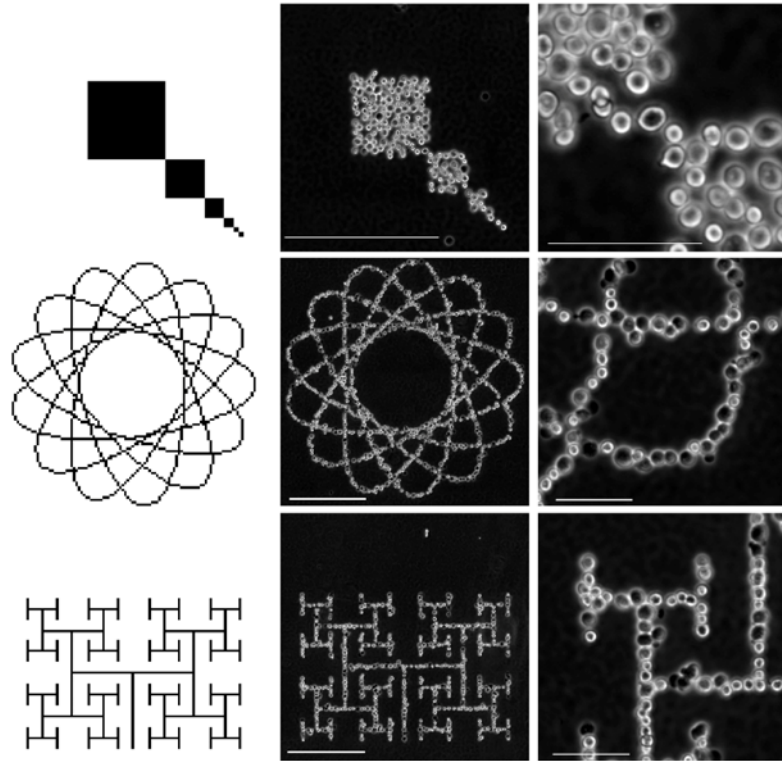


Figure 3-3. Showcase of dense, circular, and fractal patterns.

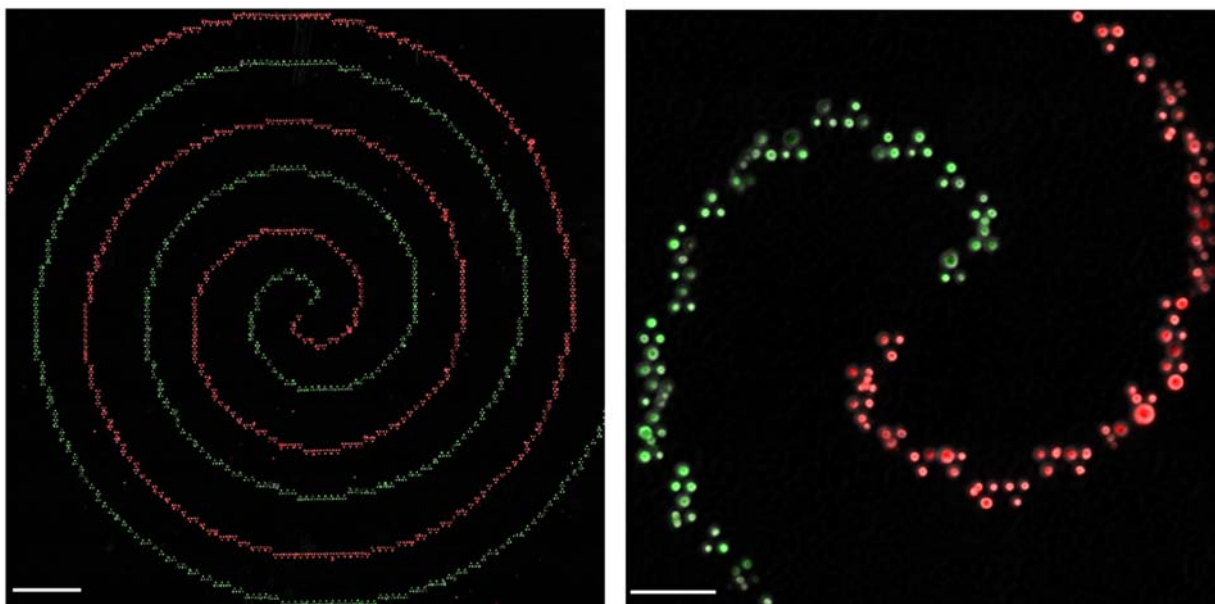


Figure 3-4. Synthesis of two-component in-register cellular pattern.

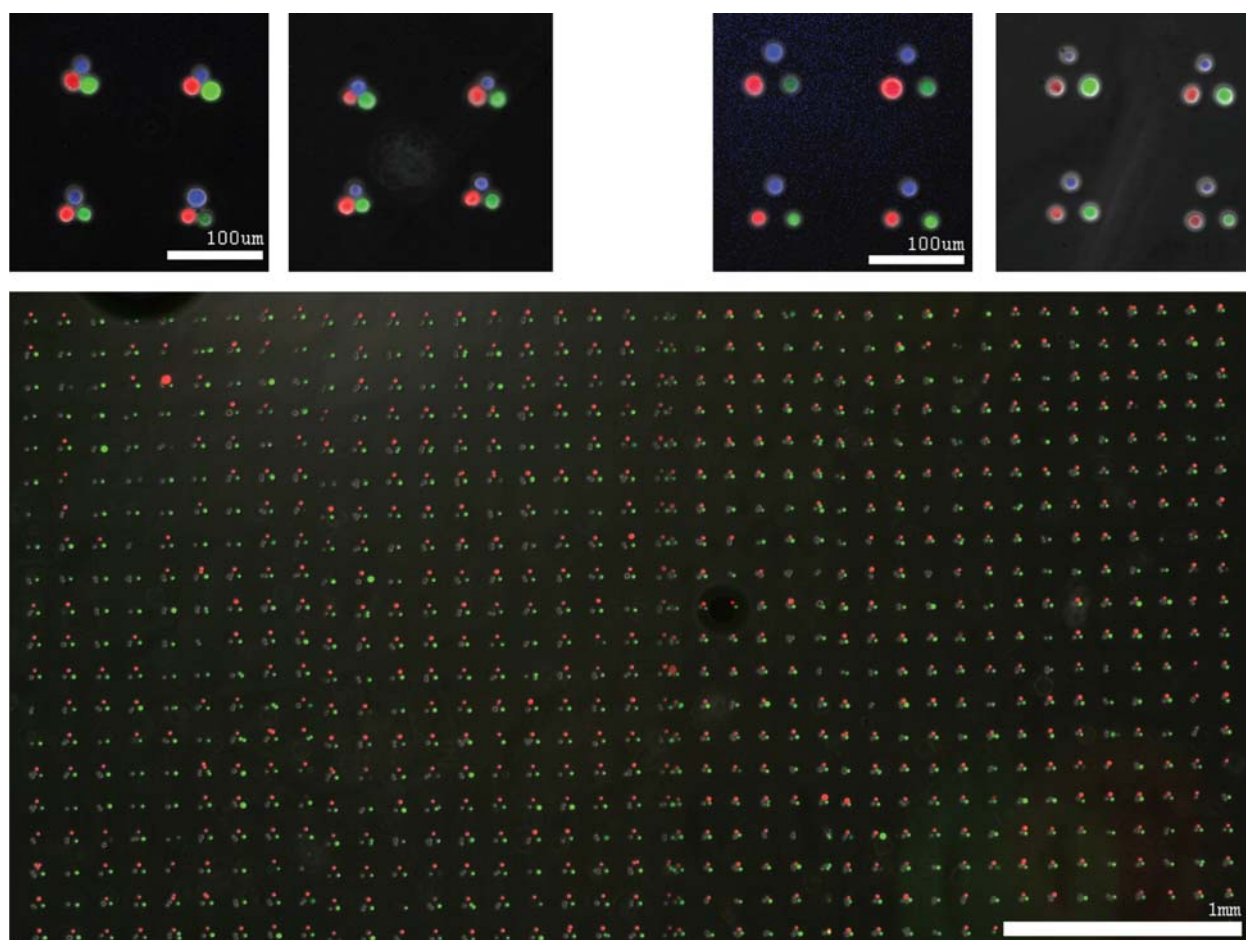


Figure 3-5. Synthesis of three-component in-register cellular pattern.

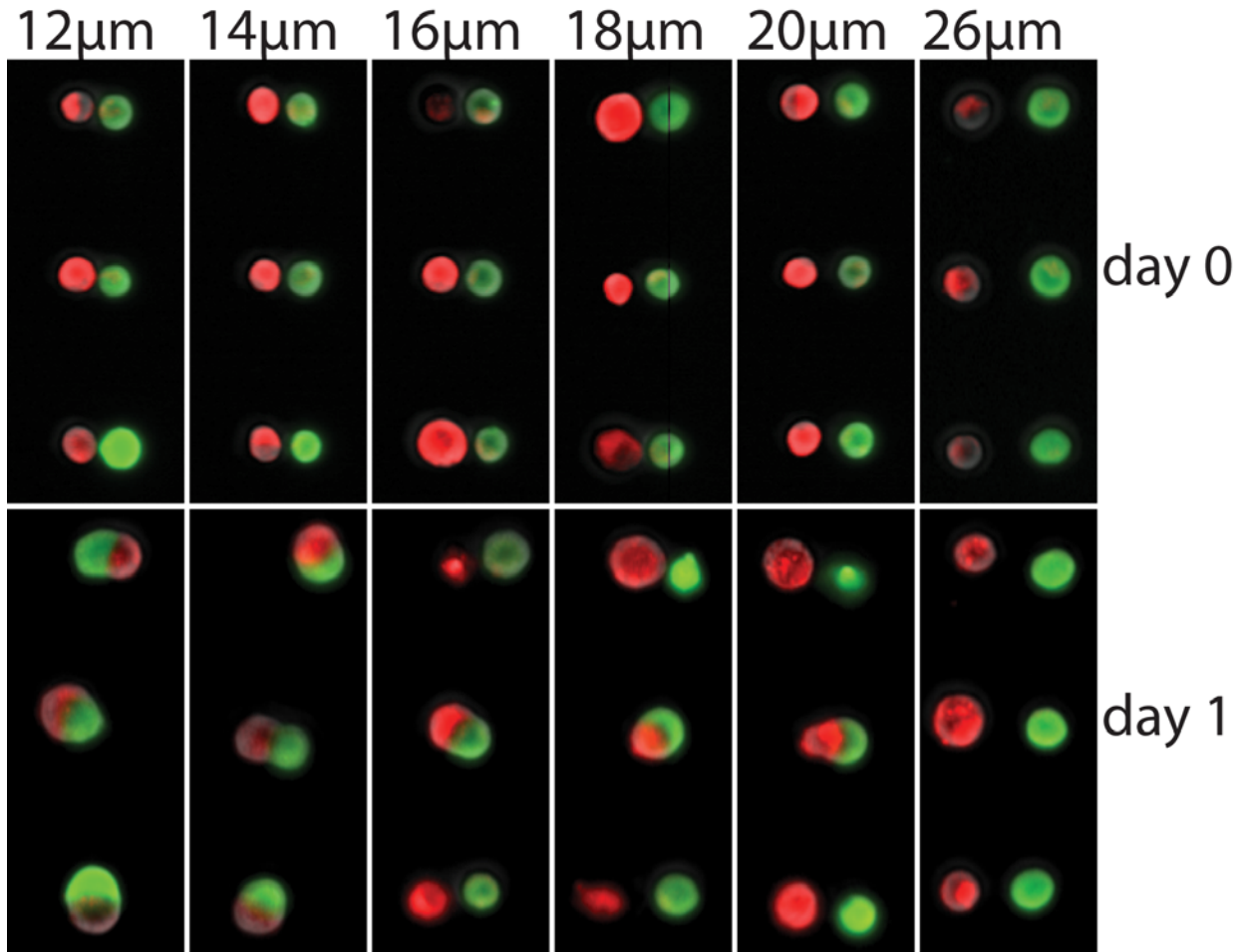


Figure 3-6. Micron-level control of cell-cell spacing. Cell pairs grown for 24 hours exhibit spacing-dependent fusion.

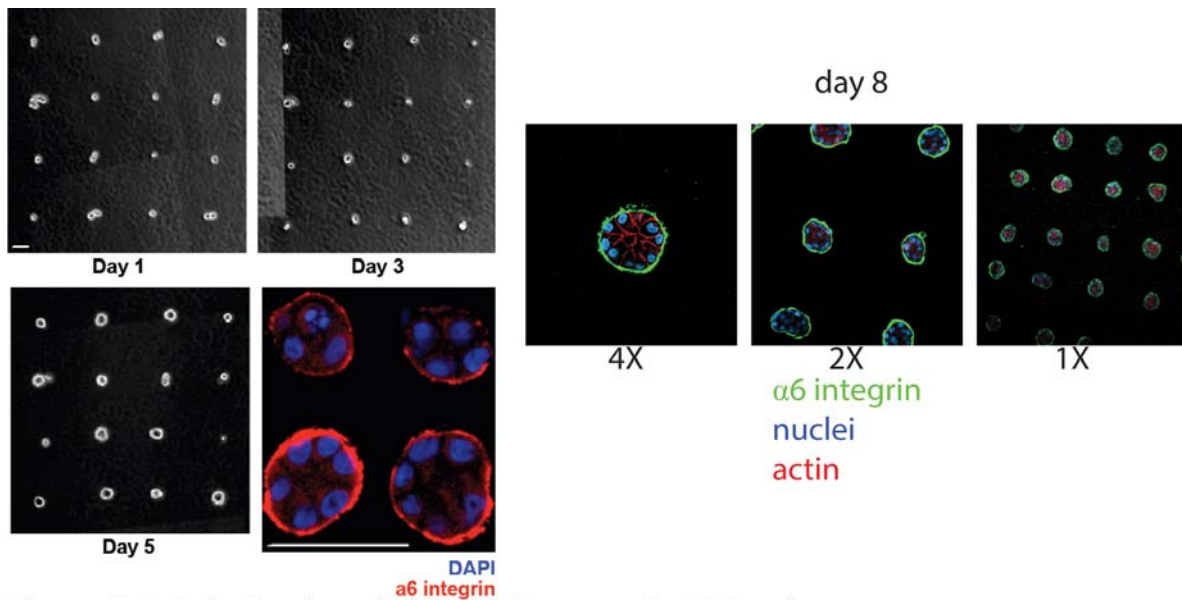


Figure 3-7. Polarization of MCF-10As grown in CPA culture.

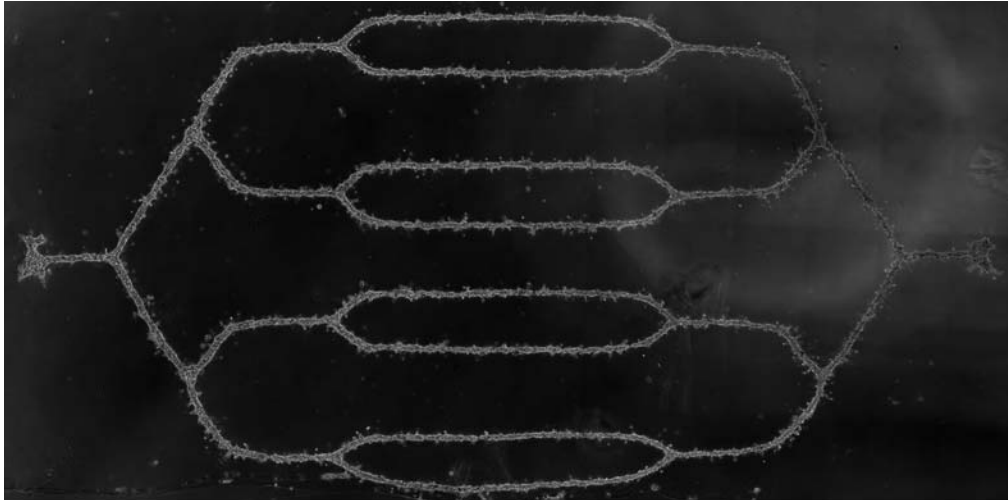


Figure 3-8. Synthesis of large-scale endothelial bed. Microtissue photographed while still embedded in flow cell, with penny for scale.

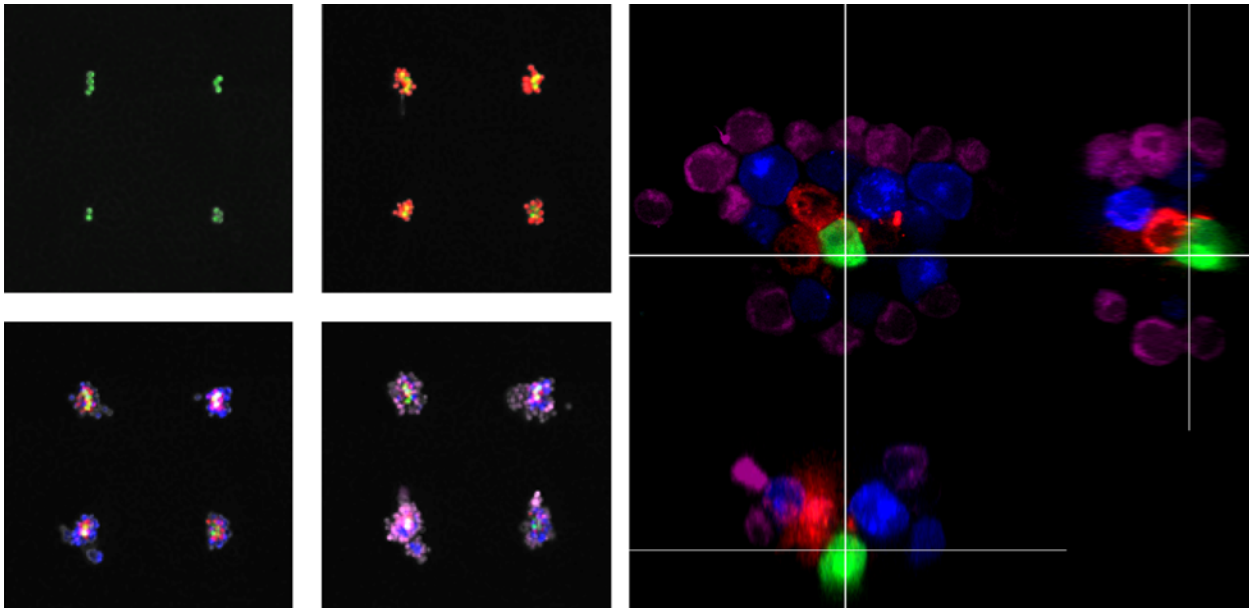
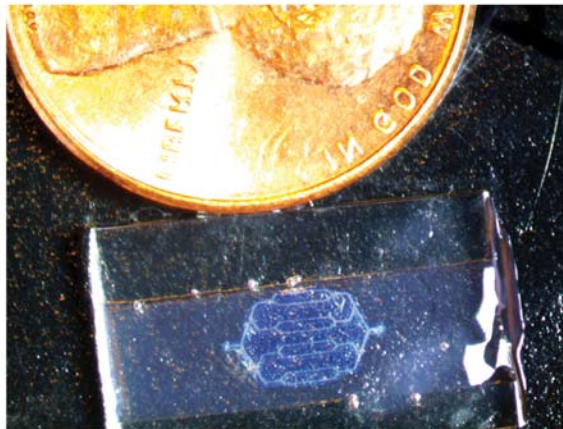


Figure 3-9. Layer-by-layer assembly of CPA cell clusters. Clockwise from top left, four successive steps of CPA grow a cell cluster. Orthogonal views at right.

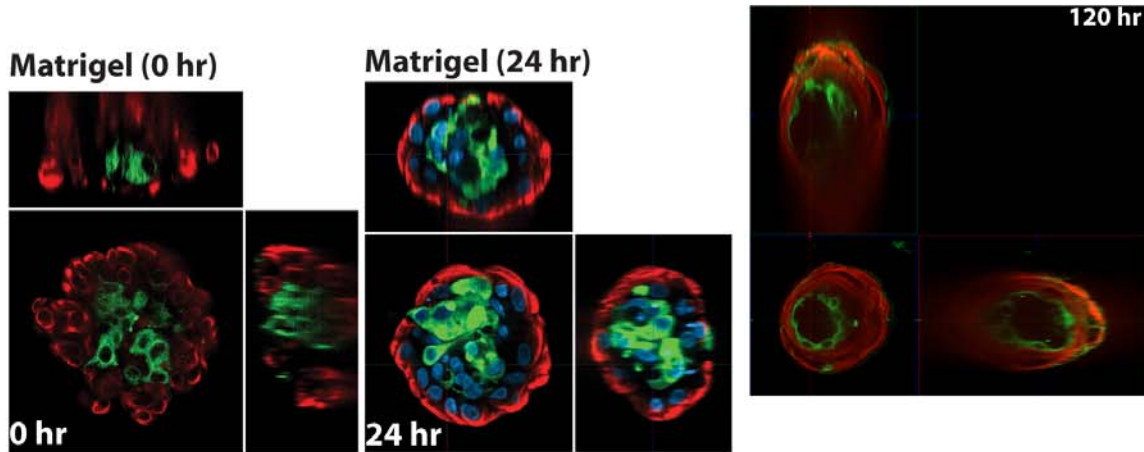
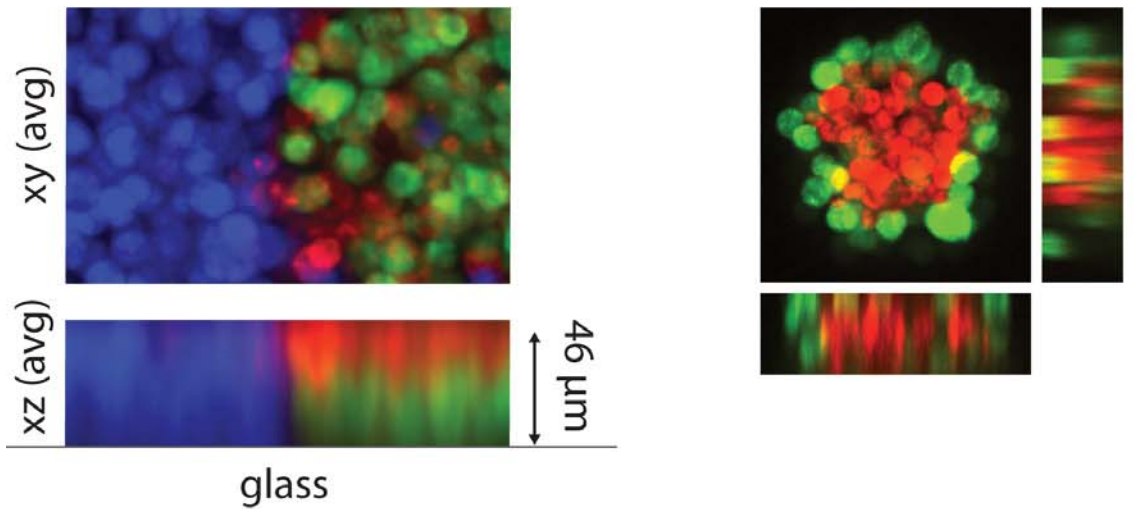
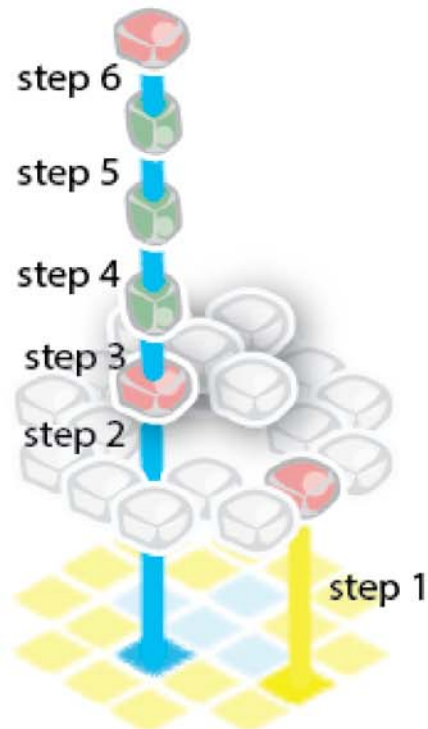


Figure 3-10. Synthesis of microtissues with defined structure along the Z-axis. Top left: a stratified microtissue with red cells positioned directly on top of green cells, with blue cells alongside. Top right: a spheroidal microtissue with red cells totally enclosed by a layer of green cells. Middle left: as top-right, but grown using HMECs that form a bilayered structure after 24hrs culture. Middle right: as middle-left, but grown for 120hrs. At this time point, lumenization of the microtissue was evident. At right: a diagram of the scheme for synthesis of totally enclosed structures.



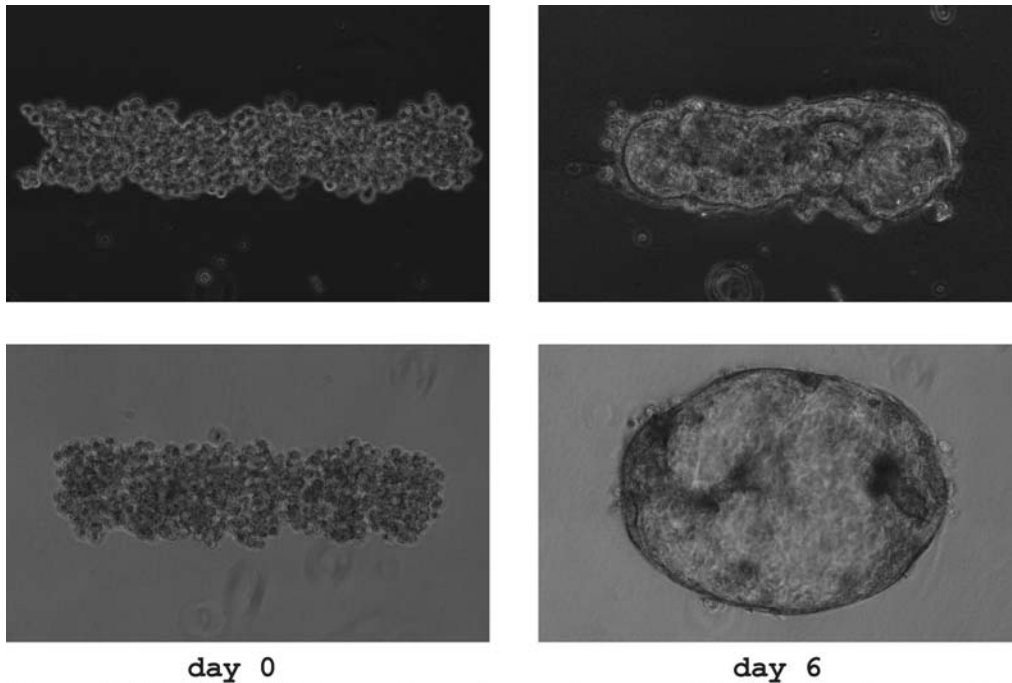


Figure 3-11. Culture-dependent shape change of Caco microtissues. At top, microtissues were grown for three days in DMEM+10% FBS followed by four days in DMEM alone. At bottom, microtissues were grown for seven days in DMEM+10% FBS.

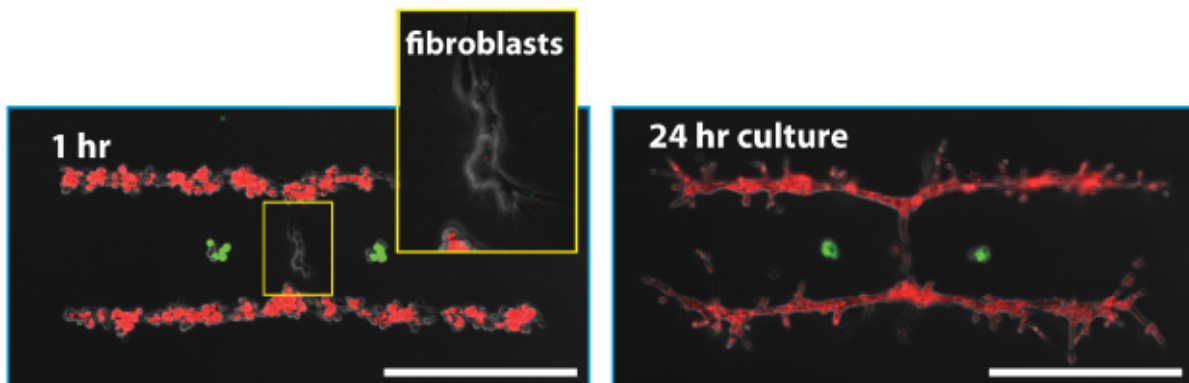
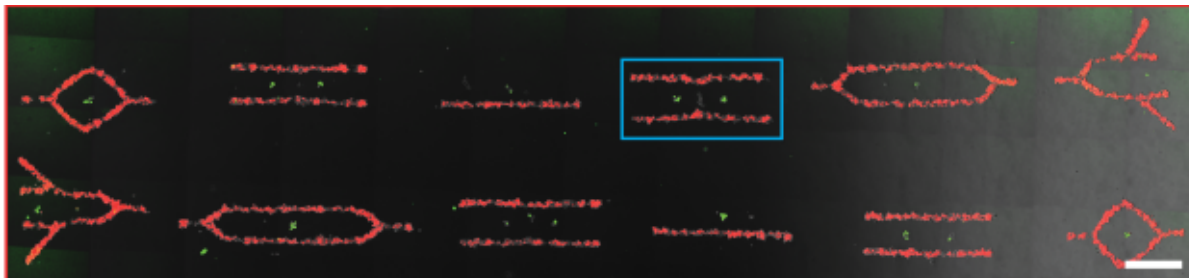


Figure 3-12. Synthesis of three-component microtissues containing multiple functional cell types. Red cells are HUVECs, green cells are MCF-10ATs, and uncolored cells are 82-6 skin fibroblasts. At top, a variety of culture patterns are visible. At bottom, condensation of the MCF-10ATs into spheroids and pulling of the HUVECs by the fibroblasts are evident.

	Surface DNA	Cell type	Cell DNA	Gel (all +40U/mL DNase)	Media	Culture Time	CPA Progression
Fig 3-1,2,3	A-amine	MCF-10A	Aprime-lipid	9 mg/mL Matrigel	10A Assay Medium	3 hours	1) 10A&Aprime
Fig 3-4,6	A-amine B-amine	MCF-10A	Aprime-lipid Bprime-lipid	9 mg/mL Matrigel	10A Assay Medium	24 hours	1) 10A&Bprime 2) 10A&Aprime
Fig 3-5	A-amine B-amine D-amine	MCF-10A	Aprime-lipid Bprime-lipid Dprime-lipid	9 mg/mL Matrigel	10A Assay Medium	24 hours	1) 10A&Dprime 2) 10A&Bprime 3) 10A&Aprime
Fig 3-7	A-amine	MCF-10A	Aprime-lipid	9 mg/mL Matrigel	10A Assay Medium	192 hours	1) 10A&Aprime
Fig 3-8	A-amine	HUVEC HUVEC	Aprime-lipid A-lipid	6.1 mg/mL Matrigel + 2.1mg/mL collagen I	HUVEC Culture Medium	24 hours	1) HUVEC&Aprime 2) HUVEC&A 3) HUVEC&Aprime 4) HUVEC&A
Fig 3-10, t.l.	A-amine F-amine	MCF-10A	Aprime-lipid A-lipid Fprime-lipid F-lipid	n/a	n/a	n/a	1) 10A&Fprime (blue) 2) 10A&Aprime (red) 3) 10A&F (blue) 4) 10A&A (red) 5) 10A&Fprime (blue) 6) 10A&Aprime (red) 7) 10A&F (blue) 8) 10A&A (green) 9) 10A&Fprime (blue) 10) 10A&Aprime (green) 11) 10A&F (blue) 12) 10A&A (green)
Fig 3-10, t.r.	A-amine F-amine	MCF-10A MCF-10A CHO CHO	Fprime-lipid Aprime-lipid Aprime-lipid A-lipid	9 mg/mL Matrigel	M87A Medium	24 hours	1) 10A&Fprime 2) 10A&Aprime 3) CHO&A 4) CHO&Aprime 5) CHO&A 6) 10A&Aprime
Fig 3-10, b.l.	A-amine B-amine	HMEC-MEP HMEC-MEP HMEC-LEP HMEC-LEP	Bprime-lipid Aprime-lipid Aprime-lipid A-lipid	6.1 mg/mL Matrigel + 2.1mg/mL collagen I	M87A Medium	24 hours	1) MEP&Bprime 2) MEP&Aprime 3) LEP&A 4) LEP&Aprime 5) LEP&A 6) MEP&Aprime
Fig 3-10, b.r.	A-amine B-amine	HMEC-MEP HMEC-MEP HMEC-LEP HMEC-LEP	Bprime-lipid Aprime-lipid Aprime-lipid A-lipid	9 mg/mL Matrigel	First 48 hrs: M87A Medium Next 72 hrs: 2:1:1 MEBM:DMEM:F12	120 hours	1) MEP&Bprime 2) MEP&Aprime 3) LEP&A 4) LEP&Aprime 5) LEP&A 6) MEP&Aprime
Fig 3-11	A-amine	CACO CACO	Aprime-lipid A-lipid	6.1 mg/mL Matrigel + 2.1mg/mL collagen I	First 72 hrs: DMEM+10% FBS Next 72hrs: either DMEM+10% FBS or DMEM	144 hours	1) HUVEC&Aprime 2) HUVEC&A 3) HUVEC&Aprime 4) HUVEC&A
Fig 3-12	A-amine B-amine D-amine	HUVEC HUVEC MCF-10AT MCF-10AT 71C	Aprime-lipid A-lipid Bprime-lipid B-lipid Dprime-lipid	6.1 mg/mL Matrigel + 2.1mg/mL collagen I	M87A Medium	24 hours	1) 71C&Dprime 2) HUVEC&Aprime 3) HUVEC&A 4) HUVEC&Aprime 5) 10AT&Bprime 6) 10AT&B

Table 3-1. Chart of experimental conditions.

3-2 Using CPA to observe tethered suspension cells.

One of the most straightforward applications of CPA is to forego 3D tissue synthesis and simply use the process to tether suspension cells to a solid surface for easy observation. The strength of DNA hybridization means that a 10 μm -wide cell can be tethered to a 4 μm -wide DNA spot, allowing the majority of the cell membrane to exhibit untethered dynamics. Depending on the type of DNA used, a cell anchored in this manner can be kept stable on a solid surface for up to a couple days, or longer in the presence of a DNase inhibitor such as aurintricarboxylic acid.

We exploited these properties of DNA hybridization to observe the membrane dynamics of arrays of Jurkat leukocytes over an hour-long period. Owing to their leukocyte lineage, Jurkats exhibit extensive membrane dynamics, with various protrusions extending and retraction on the time scale of seconds. When Jurkats are immobilized, these dynamics can be observed over the time scale of hours. Figure 3-13 summarizes the findings. First, there exists heterogeneity among the extent of dynamics exhibited by these Jurkat cells, and the degree of heterogeneity can be reduced by addition of the drug pair 12-o-tetradecanoylphorbol-13-acetate (PMA) and ionomycin. Furthermore, this drug pair not only reduces heterogeneity but also increases the overall quantity of cell protrusions, or "microspikes," exhibited by the cells. Figure 3-14 shows key frames of several representative Jurkats. An additional phenomenon is that drugging the cells with latrunculin causes the standard membrane dynamics to cease. Instead, long, single protrusions, referred to as "microtentacles," emerge from the cells. Drugging with latrunculin the completely different cell type MCF-10A, a mammary epithelial cell line, revealed this same microtentacle phenomenon. It is my assertion that these structures are tubulin-based and have extended beyond the cell due to the absence of restraining cortical tension. This is substantiated

by the observation that treatment of cells with both latrunculin and nocodazole, an inhibitor of microtubule polymerization, prevents both the microspikes and the microtentacles from forming. Stuart Martin at the University of Maryland noticed the resemblance of these structures to what he observes on suspension-phase epithelial cells, such as those found circulating in blood and implicated in the invasion of circulating cancer cells from the blood into tissue. The Martin lab previously had difficulty observing their target cells, generally relying on trapping epithelial cells in agarose microwells to keep them both unanchored but also stationary for observation. Using CPA, our collaborators in the Martin lab were able to reliably observe microtentacle formation for extended periods on their cells of interest, greatly facilitating their data collection.

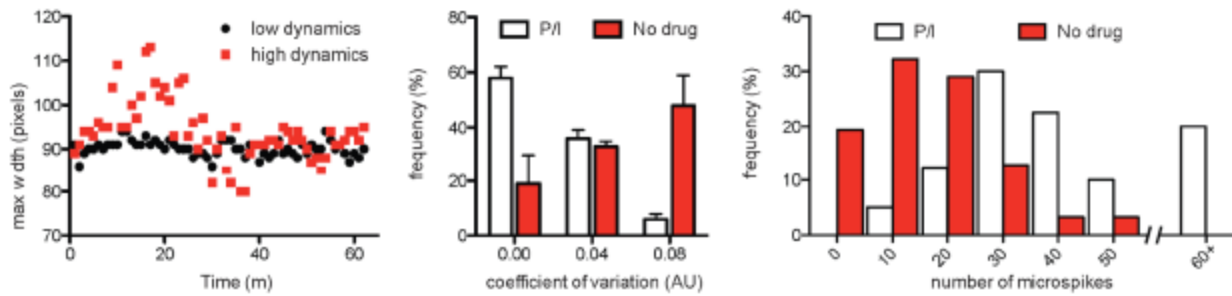


Figure 3-13. Dynamics of CPA-tethered Jurkat cells. At left, individual cells are tracked over an hour period, distinguishing cells with intrinsically high dynamics from low. Center, treating cells with PMA+ionomycin reduced variability among cells. At right, this reduced variability translated into a uniformly increased number of microspikes.

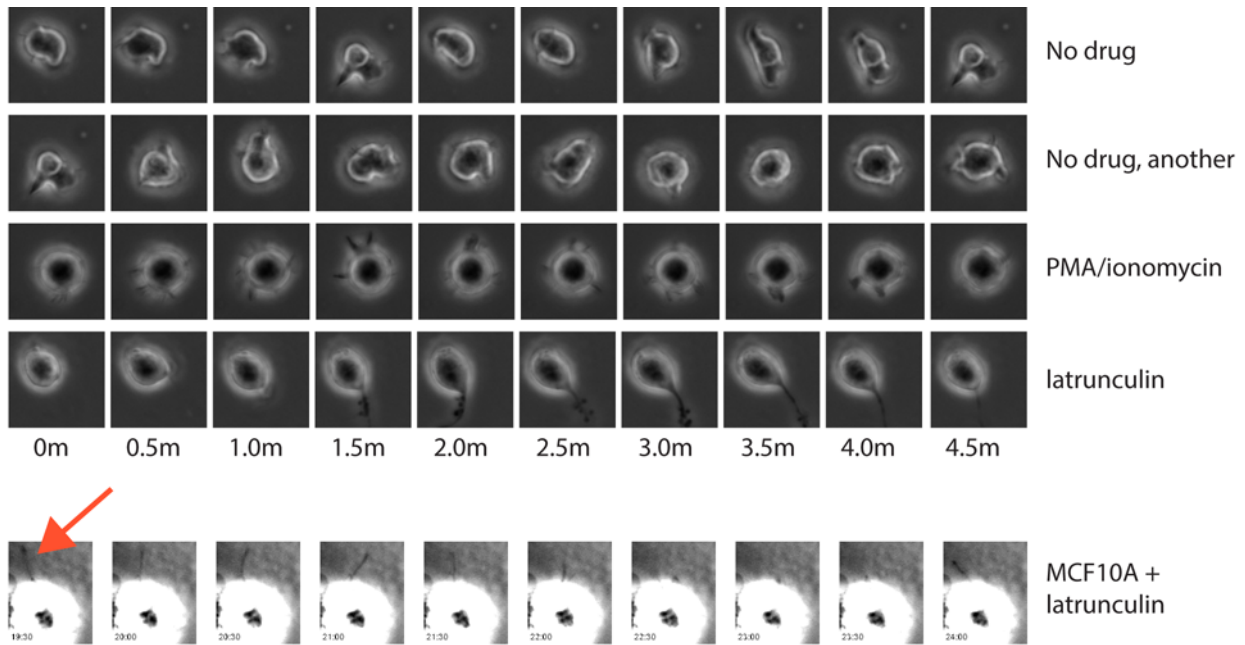


Figure 3-14. Key frames for movies of CPA-tethered cells. Jurkat cells, treated either with latrunculin, PMA/ionomycin, or no drug, are shown over a five-minute period. MCF-10As are shown over the same period.

3-3 On the behavior of fibroblasts in CPA culture.

I performed a variety of experiments analyzing the behavior of CPA-patterned fibroblasts in 3D culture. Fibroblasts are an interesting candidate cell type because they have the capacity to change the environment around them by the production, degradation, and rearrangement of collagen. Their action provides a key structural component of tissue stroma.

My first experiments with fibroblasts aimed to find media and gel conditions in which fibroblasts would grow according to their templated pattern across days-long culture. My first observation is that the fibroblast cell line I was using, human telomerase-immortalized skin fibroblasts (line 82-6), failed to thrive in gels lacking collagen. Furthermore, the behavior of the fibroblasts varied depending on the media provided. Cultured in their growth medium, DMEM + 10% FBS, the fibroblasts would branch and extend in every direction in 3D culture, regardless of the geometry with which they were patterned. As the concentration of serum was brought down, the fibroblasts would tend more-and-more to extend only along the axis with which they were patterned. I found DMEM + 3.3% FBS to be a condition with which the fibroblasts would conform to their pattern while still providing enough serum for them to thrive.

With the general goal of trying to construct tissues containing a combination of fundamentally different cell types, I produced fibroblast/epithelial microtissue arrays in which lines of fibroblasts and epithelial cells were arranged with varied orientation and density (Figure 3-15). A line of fibroblasts, on their own, when grown in the aforementioned media and gel conditions, would undergo a stereotyped progression in week-long culture: first the cells would condense into a round mass, then they would subsequently refill the space occupied by their original

pattern then extend beyond it (Figure 3-16). During this extension phase, patterned fibroblasts would exert effects on the surrounding gel. Figure 3-17 shows how fibroblasts can distort the shape of the matrix around them, presumably by rearrangement of the surrounding collagen. The magnitude of this phenomenon appeared to depend on both the number of fibroblasts and the spacing between them. Figure 3-18 showcases a couple of interactions between fibroblasts and epithelial cells: first, that fibroblasts can induce in epithelial spheroids the same shape change seen in 3-17's air bubble, and second that fibroblasts can seemingly destabilize spheroids, permitting the escape of epithelial cells if the fibroblasts come into contact.

A simple behavior that I analyzed extensively was the translocation of epithelial spheroids by lines of fibroblasts. In the above paragraph, I described how spheroids in-between two fibroblast lines can become distorted. However, if only one fibroblast line is present, the more typical outcome is movement of the spheroids towards the fibroblasts over time. This behavior depends on the relative orientation between the fibroblasts and the spheroids, and is shown in Figure 3-19. In short, the angle between the axis of the fibroblasts and the position of the spheroid seems to be the critical factor impacting translocation magnitude. When a box of spheroids fully encompasses a fibroblast line, spheroids that are near the fibroblasts but not intersecting their axis exhibit little to no translocation.

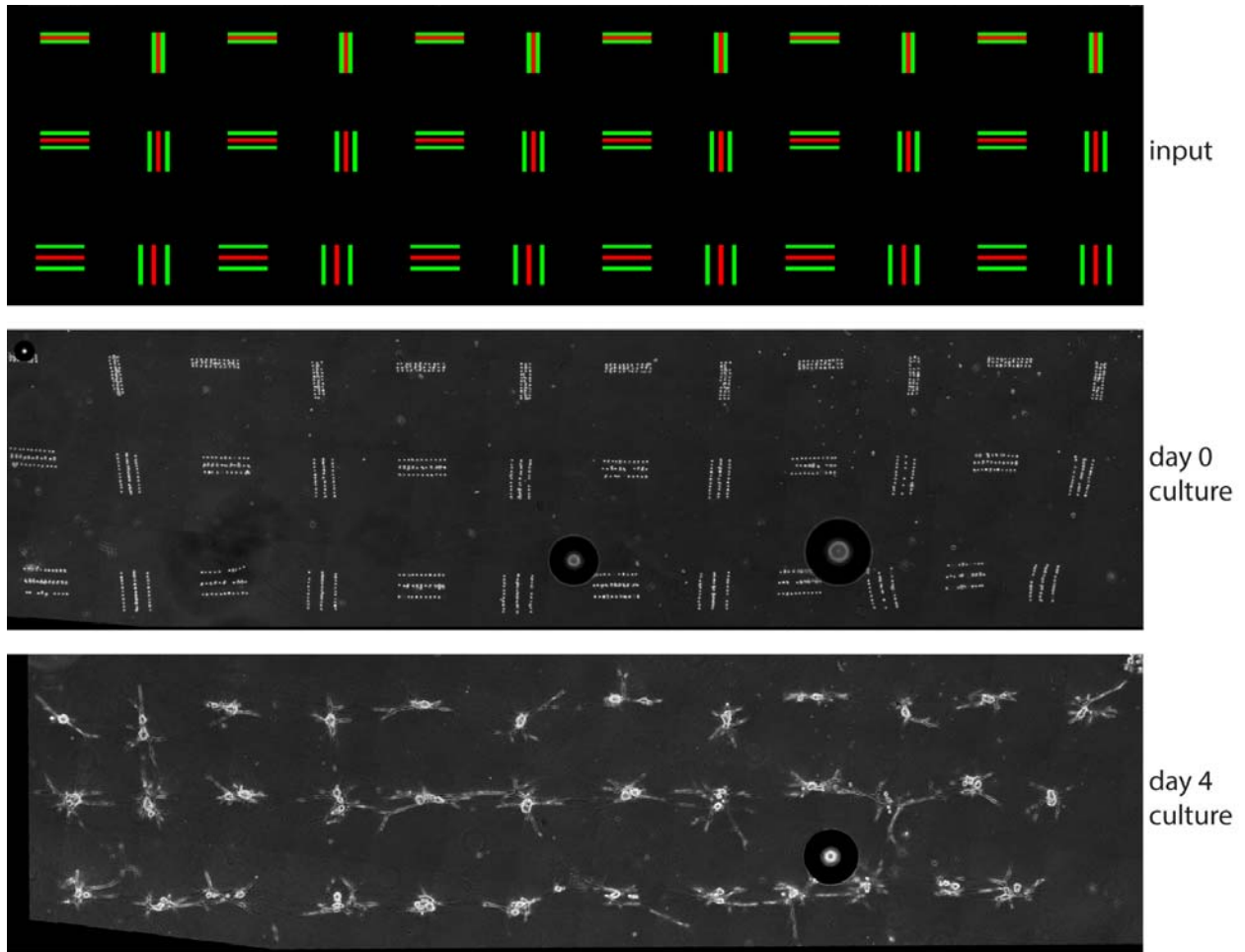


Figure 3-15. Fibroblast/epithelial microtissue array. Top, a variety of spacings and orientations are designed, with epithelial cells occupying green pixels and fibroblasts red pixels. Center, the pattern as a 3D microtissue array, and bottom, the array after several days' growth.

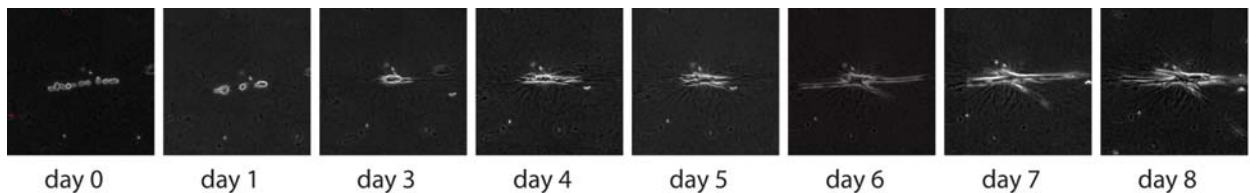


Figure 3-16. Time evolution of cultured fibroblast lines. A one-cell-wide line of fibroblasts is patterned. By day 3, it has condensed into a single round mass. By day 5, this mass has extended to approximately fill the original patterned space. By day 6, significant extension has occurred beyond the original pattern, oriented primarily along the axis of initial patterning.

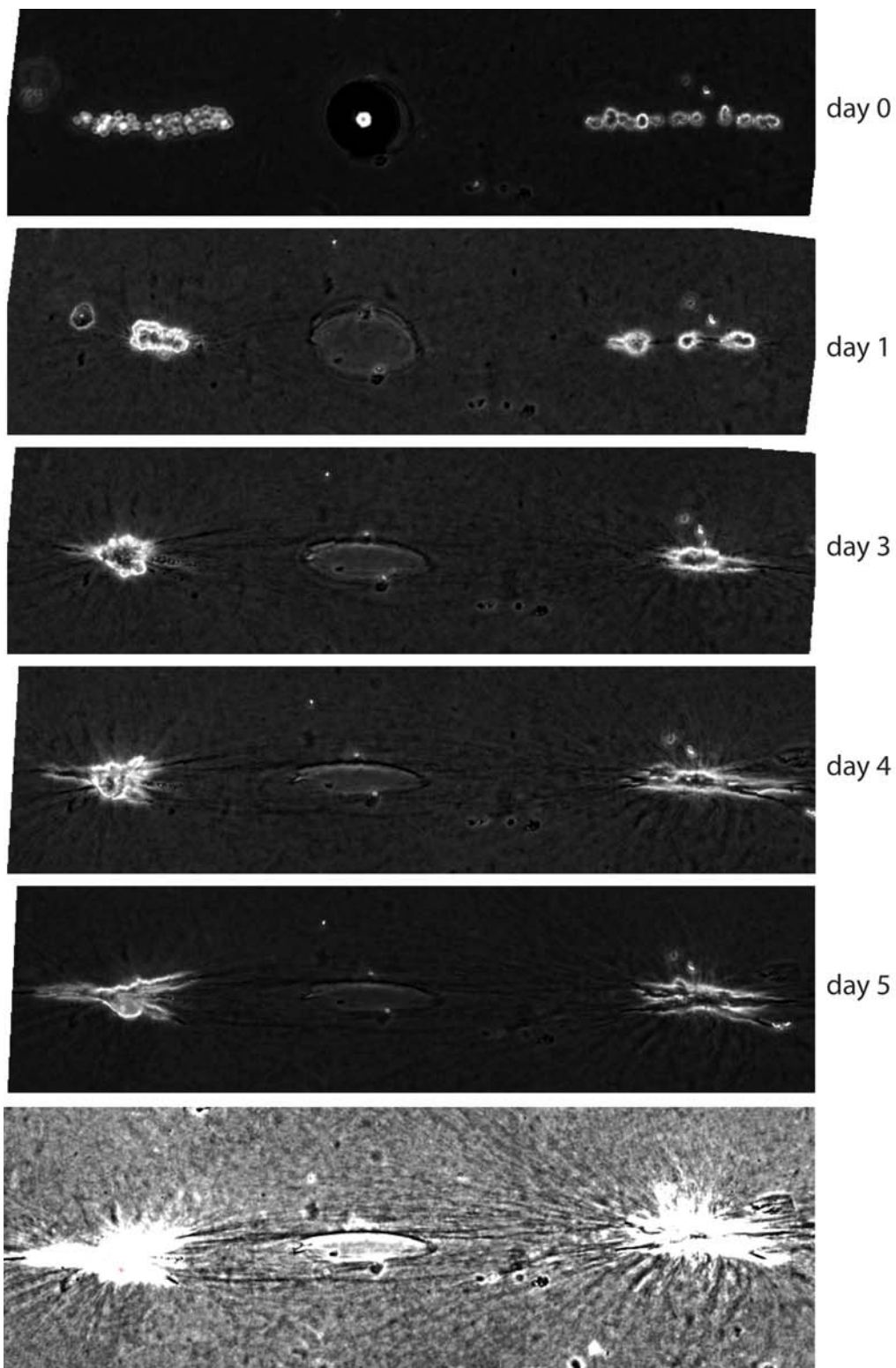
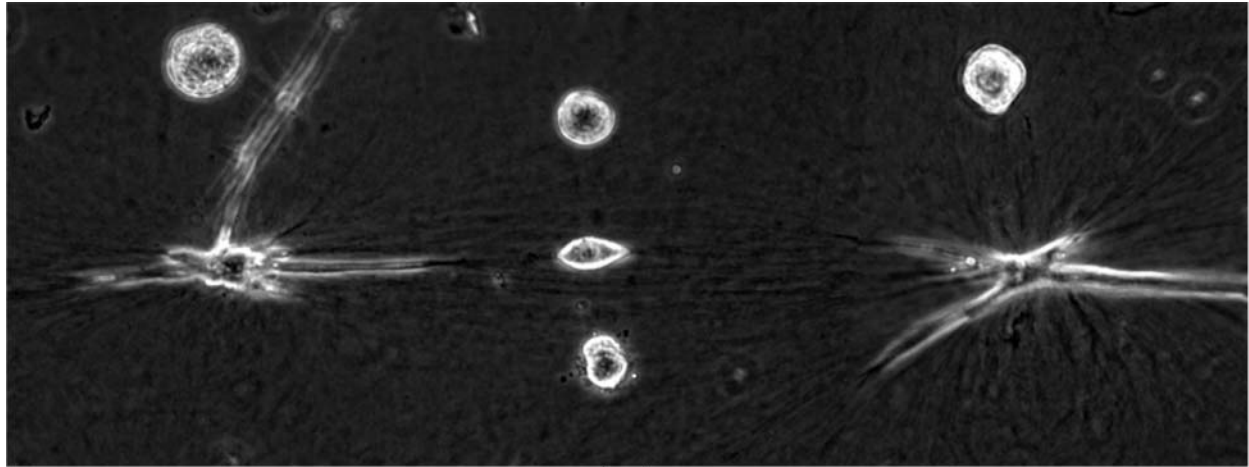
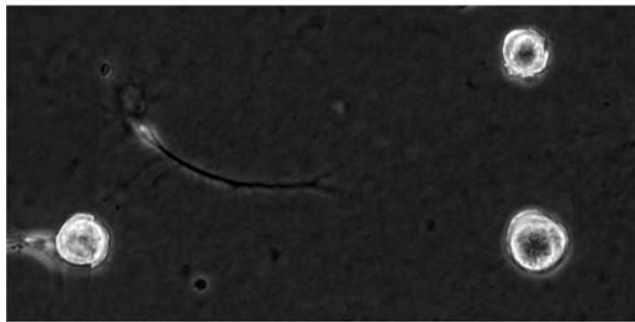


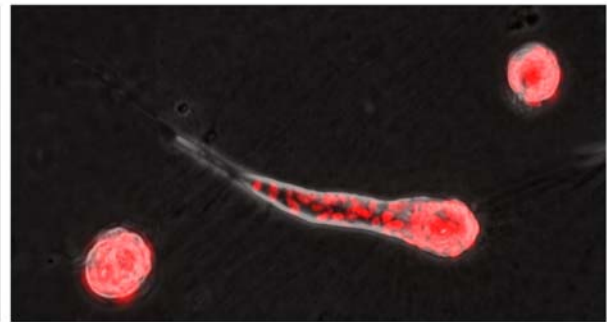
Figure 3-17. Gel deformation by patterned fibroblasts. An air bubble fortuitously formed between two fibroblast lines. Across five days, witness the deformation of the initially spherical cavity into an ellipsoid. At bottom, a high-contrast view of the day 5 image, showing stress lines traversing the hydrogel.



day 4



day 3



day 6

Figure 3-18. Interactions between fibroblasts and epithelial cells. Top, analogous to the behavior seen in 3-17, fibroblast lines distort the shape of epithelial cells between them. Bottom, fibroblasts appear to trigger the escape of cells from an epithelial spheroid (epithelial cells shown with a red overlay).

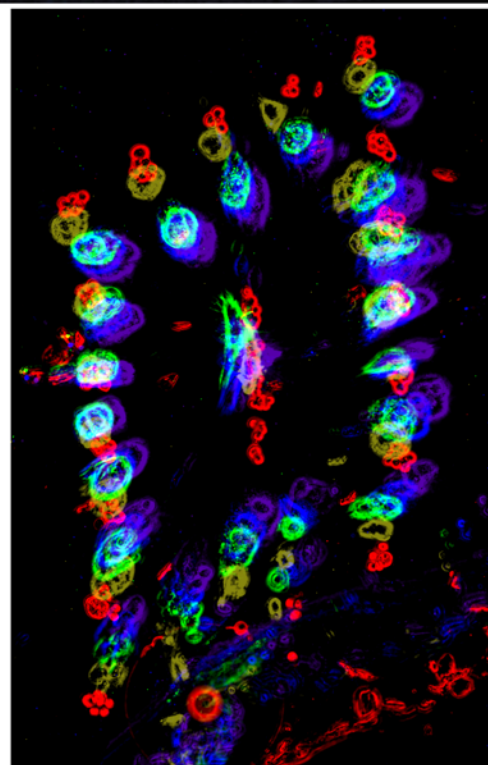
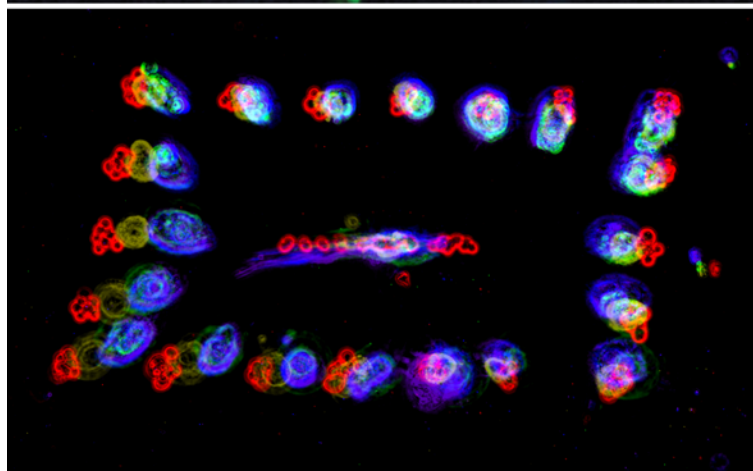
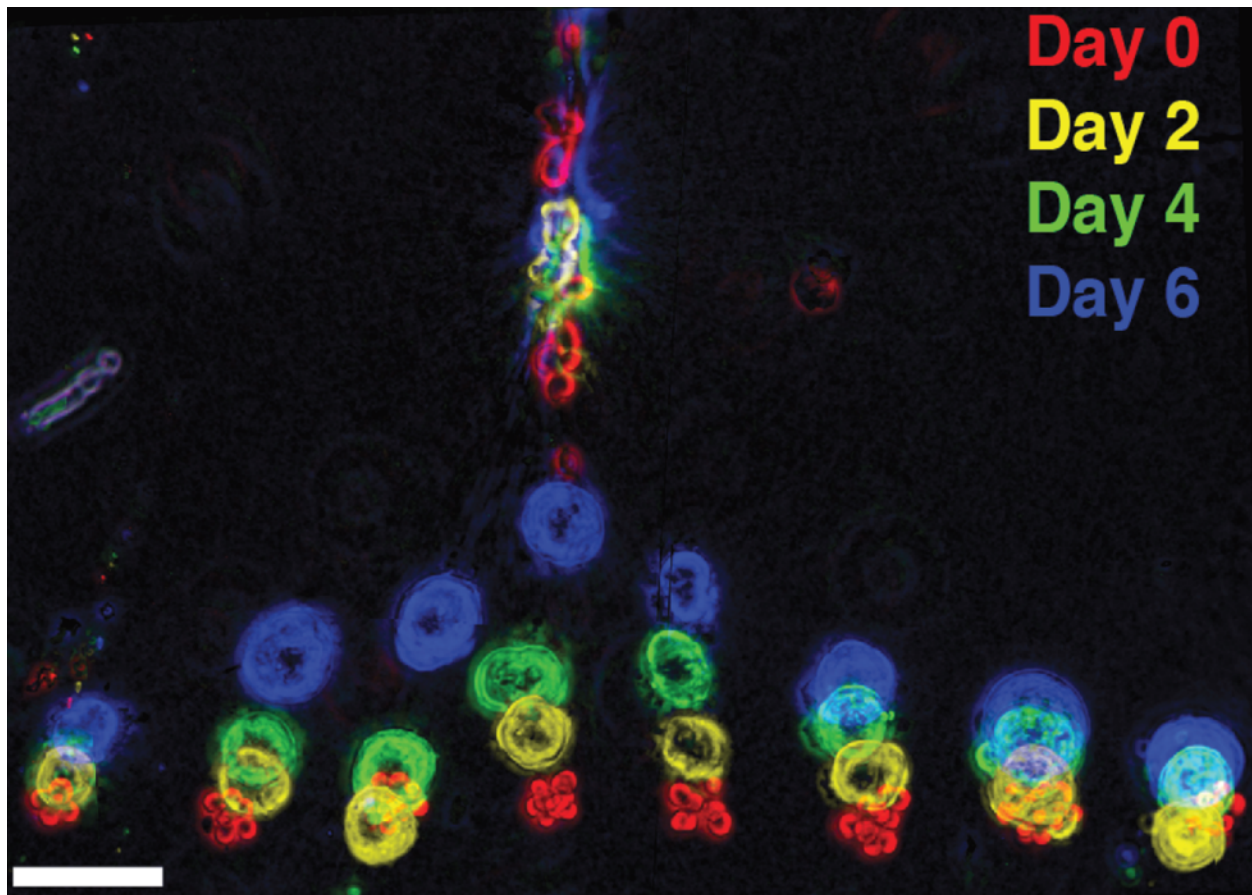


Figure 3-19. Translocation of spheroids by aligned fibroblasts. Above, fibroblasts were patterned in a line with clusters of epithelial cells aligned perpendicularly. Across week-long culture, the translocation of the spheroids towards the fibroblasts varied in an angle-dependent manner. Below, fibroblasts were patterned with clusters of epithelial cells on all sides.

3-4 Branching morphogenesis in CPA culture.

A common structural motif in mammalian biology is the branching network, as seen in the lungs, circulatory system, and mammary gland. This section shows that branching morphogenesis can be simulated and controlled in CPA culture.

Two related mammary epithelial cell lines, MCF-10A and MCF-10AT, are commonly used. MCF-10As are non-malignant but immortal, and MCF-10ATs are H-Ras^{V12}-transformed³³. MCF-10As, when grown from single cells, tend to growth arrest in 3D culture, whereas MCF-10ATs arrest incompletely. Furthermore, if grown in appropriate matrix, which in my case was Matrigel supplemented with collagen I, MCF-10ATs will form branching tubular structures. Using CPA, MCF-10As and MCF-10ATs are patterned together in a contiguous structure. This experiment is shown in Figure 3-20, where tubes composed of both MCF-10As (red) and MCF-10ATs (green) were synthesized by CPA. After the tissues were grown for several days, they exhibited branching specifically where the MCF-10ATs were present. This alone would be fairly trivial, seeing as MCF-10ATs can undergo branching on their own, but what is notable is that the MCF-10As are pulled into the branching structures as well, which they would not be competent to do on their own. In this manner, not only the position of branch points can be controlled but also otherwise incompetent cells can be impelled to participate in branching.

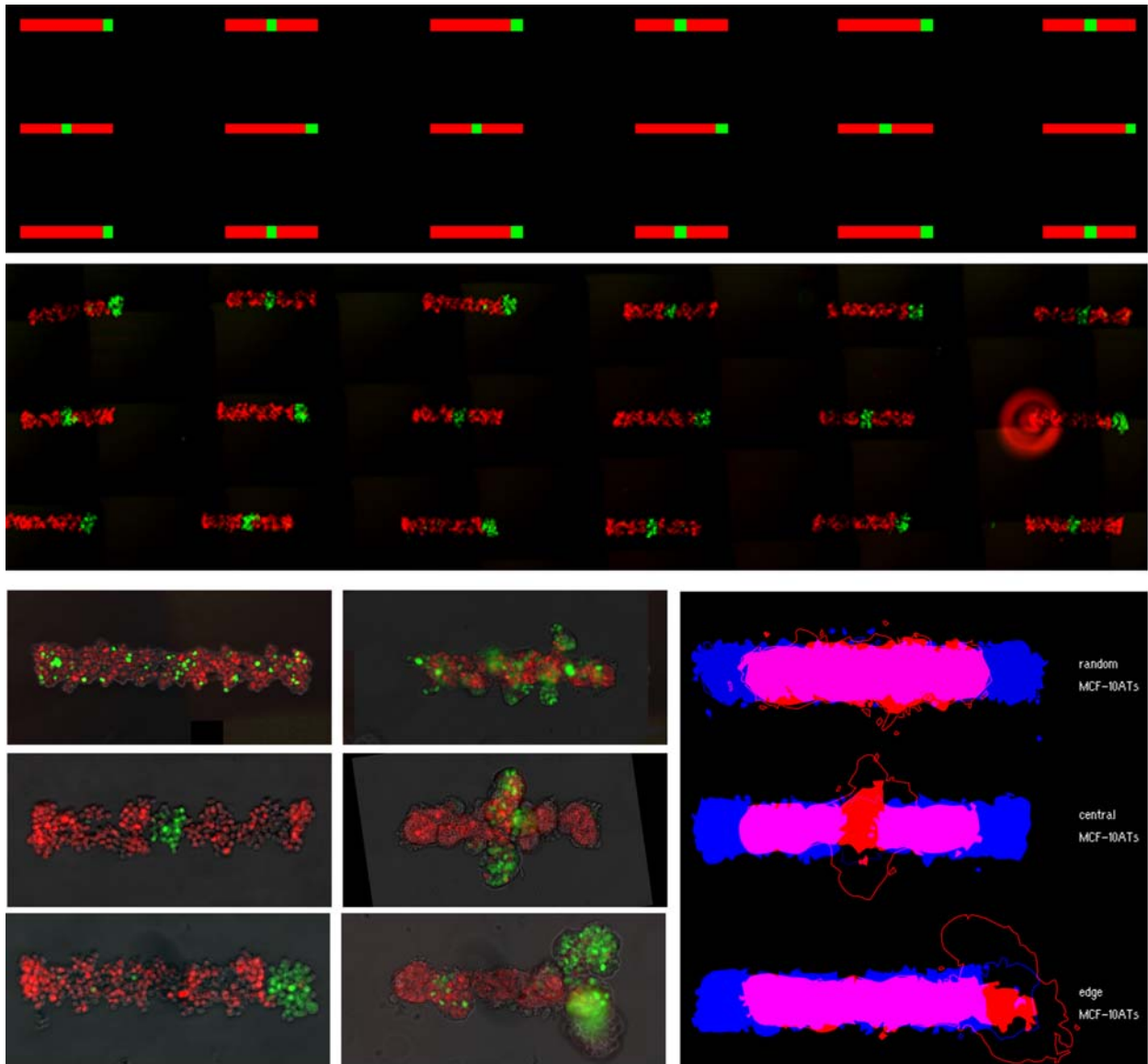


Figure 3-20. Branching morphogenesis of heterotypic MCF10A/T tubes. Above, full-field images of the input pattern and day 0 3D-CPA microtissue array. Below, at left, day 0 images of microtissues with MCF-10ATs positioned randomly, centered, or on the edge. Below, middle, the same microtissues at day 3 of culture. Below, at right, plots showing the average contour of all microtissues at day 0 (blue) and day 3 (red).

4 THE WAY FORWARD

4-1 Technical advances to facilitate adoption and reproducibility of CPA.

When it comes to developing any technology, one of the most important facets is to determine whether this technology can be widely adopted. There are myriad technologies, especially in biotechnology, which are enabling of new capabilities to researchers, but which are grounded in uselessness because of their inability to be adopted, either because of the technical requirements or expense required. To make a technology that will endure and spread, it is essential to mitigate these factors.

Towards that end, there are several favoring to CPA. First, there is the fact that the only essential reagent is lipid-DNA, which can be produced at low cost and with relative ease. Second, there is the fact that there is only one major capital investment required, which is the Nano eNabler. Depending on the patterns that the user wishes to pursue, this instrument may not even be required, with substitution by other, cruder technologies being quite possible while still useful.

One of the most important advances that is needed in the CPA workflow is a faster, more consistent way to produce patterns. Microscale direct writing permits the rapid design of new patterns, but its speed is limited when actually creating those patterns. The problem is fundamental and intractable: microscale direct writing prints all its features one-at-a-time, whereas other techniques such as photolithography print its features all-at-once. Unfortunately, traditional "all-at-once" techniques do not have the rapid print-test cycle or facile multiplexing capabilities as microscale direct writing. However, I see a possible solution, and that solution is maskless photolithography.

Maskless photolithography is a technology which has been with us for several years. It is simple in principle, using a projector to beam a pattern onto the surface of interest rather than using a photomask. Digital micromirror devices have increased the resolution and power of such techniques, especially when using light in the visible range. It would be straightforward to construct a device which shined light, of the appropriate wavelength, onto a chemically activated glass slide on which a reaction occurs specifically where the light is shining. If the reagents can be switched out while the slide and projector remain in fixed position relative to one another, then multiplexing can be trivially achieved. One possible chemistry for this method would be to have a surface displaying nitrobenzyl-cysteine, and to react that surface with maleimide-DNA. But, any photoactivatable or photocleavable reagent that could be bonded to glass could be appropriate for this technique. If maskless photolithography were to work, the time to produce patterns would drop from hours to minutes. Furthermore, feature-dense patterns such as wide tubes could become patternable in the exact same amount of time, whereas they take prohibitively long to pattern with existing techniques.

A second point is that the amount of time required for CPA during live-cell manipulations needs to be minimized. There is a wide variety of mammalian cells out there, and they have varying degrees of tolerance to manipulation. In general, I found that the most interesting cells are the most delicate cells - primary cells, unsuited to suspension, unsuited to prolonged manipulation. As I write this, it takes 10-15 minutes for each round of CPA. The most complex microtissues I've made have taken eight rounds of CPA. This hour or two of suspension manipulations may mean nothing to cells such as MCF-10As, but it is certain death for cells such as primary cortical

neurons. In principle, this time can be reduced: DNA hybridization is fast, taking only seconds to go to completion, and there is no reason that the CPA rounds could not be correspondingly quickened. In order to accomplish this, we need a fundamentally different approach to the CPA cycles. As described in Chapter 2, a round of CPA involves waiting several minutes for cells to settle two hundred microns to the bottom of a flow cell, followed by manual pipetting to roll the cells through the flow cell and sample the surface. Essential parameters, such as the Z-position and speed of the cells, are uncontrolled and indeed difficult to even measure while performing these manipulations. The solution is to adopt automation. If the rate of flow can be controlled, such as by pump, while simultaneously the contents of the flow cell be observed by camera, then a feedback loop can be established with which the optimal flow rate can be determined to minimize the attachment time. The same is true of the settling time. As for the "cycling" outlined in chapter 2, it is sound in principle, but it has been heretofore impossible to optimize. An apparatus such as shown in Figure 4-1 should permit this sort of optimization.

There are other means to maximize the viability of delicate cell feedstocks. The temperature of all manipulations should be kept as low as possible. The most straightforward approach is to perform all manipulations on ice. Placing the flow cell apparatus onto crushed ice within an ice bucket is generally sufficient only to reach 4-6° C, as measured by an instant-read infrared thermometer. I have had success placing the apparatus instead upon a solid block of ice supplemented with sodium chloride to 10% w/w. Although the freezing point of this salt ice is -6° C, the several millimeters between the ice and flow channel tends to keep the flow channel at about 1° C.

I have also performed experiments testing the effectiveness of cold storage solutions, normally used for the preservation of human organs before transplant operations, such as HypoThermoSol or UW Cold Storage Solution. At both brief (1 hour) and prolonged (overnight) time scales, I have not observed any improvement in viability of suspension-phase MCF-10As when stored in cold storage solution versus PBS (viability measured by ethidium homodimer incorporation). I tentatively conclude that the issues limiting viability for suspension-phase cells are different than the issues limiting viability for whole human organs.

When dealing with precious cell feedstocks, not only the viability but also the number of cells can be limiting. When dealing with cell lines, it is trivial to obtain millions of cells. This is even true for primary cells as long as they can undergo several expansions. However, many desirable cell types cannot be propagated *ex vivo*. When dissociating tissue, especially when isolating scarce cell populations or when working with small tissues such as lymph nodes, it may not be possible to get more than 10,000 cells of a single type. It would be desirable to be able to undergo CPA successfully even with these low numbers. I have had success, working with collaborators in Max Krummel's lab, attaching cells to surfaces via CPA with as few as 10,000 cells of a given type. Unfortunately, I have no hard data on what was necessary to accomplish this. Presumably, sufficient recycling of cells across the surface of the patterned slide should enable attachment of such populations. An apparatus that can tune flow rates, such as the one previously shown in Figure 4-1, should be capable of performing the necessary optimizations for such cells.

Another consideration is the reliability of the 3D transfer manipulations. Success in the 3D transfer manipulations requires steady hands, sharp tweezers, rapid manipulations, and a certain degree of luck. I have been able to successfully train a handful of researchers to perform 3D transfer, but the learning curve means that for several weeks, experiments will not be reliable while someone is learning the technique. Furthermore, even with experienced users, the failure rate is non-zero. Considering that two full days of labwork, along with precious human cells, can be consumed by a tissue synthesis experiment, this failure rate is costly and frustrating. The major failure modes are summarized in Figure 4-2. Mitigation of these failure modes would be beneficial to the usefulness of CPA.

A general approach to mitigating 3D transfer failure is to simply automate unreliable steps. A device which could apply constant, reproducible force along a precise vector should be able to prevent the sorts of failures in Figure 4-2 from occurring. This is not possible with manual manipulations. However, it is possible with magnetic manipulations. Atomized steel, a readily available formulation of highly divided iron, can be mixed into PDMS to produce a flow cell responsive to magnetic fields. Fabrication of an electromagnet on a three-axis rig can permit the manipulation of this flow cell entirely by magnetic fields. While the prototype shown in Figure 4-3 has three axes controlled by knobs, a more sophisticated version of the same device could have electronically controlled rails and/or be expanded to permit simultaneous manipulation of multiple flow cells. Such manipulations have the advantages of being both smooth and precisely defined.

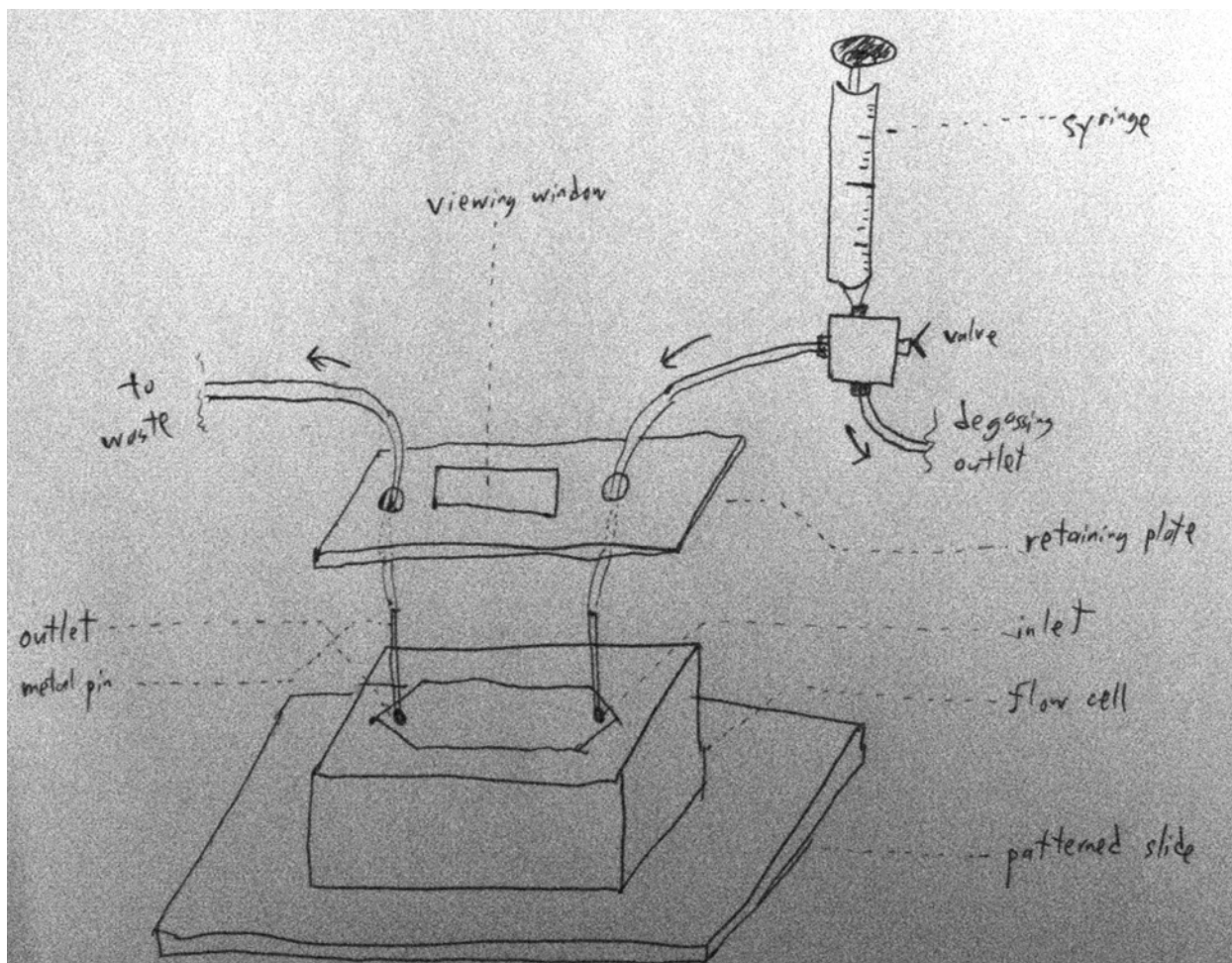


Figure 4-1. Scheme for continuous flow apparatus. Syringe-driven flow can be adapted to the same PDMS flow cells and the same patterned slides used in the current protocol. Retaining plate prevents pins from falling out. This scheme is compatible with clamped retention of the flow cell by application of force to the retaining plate.

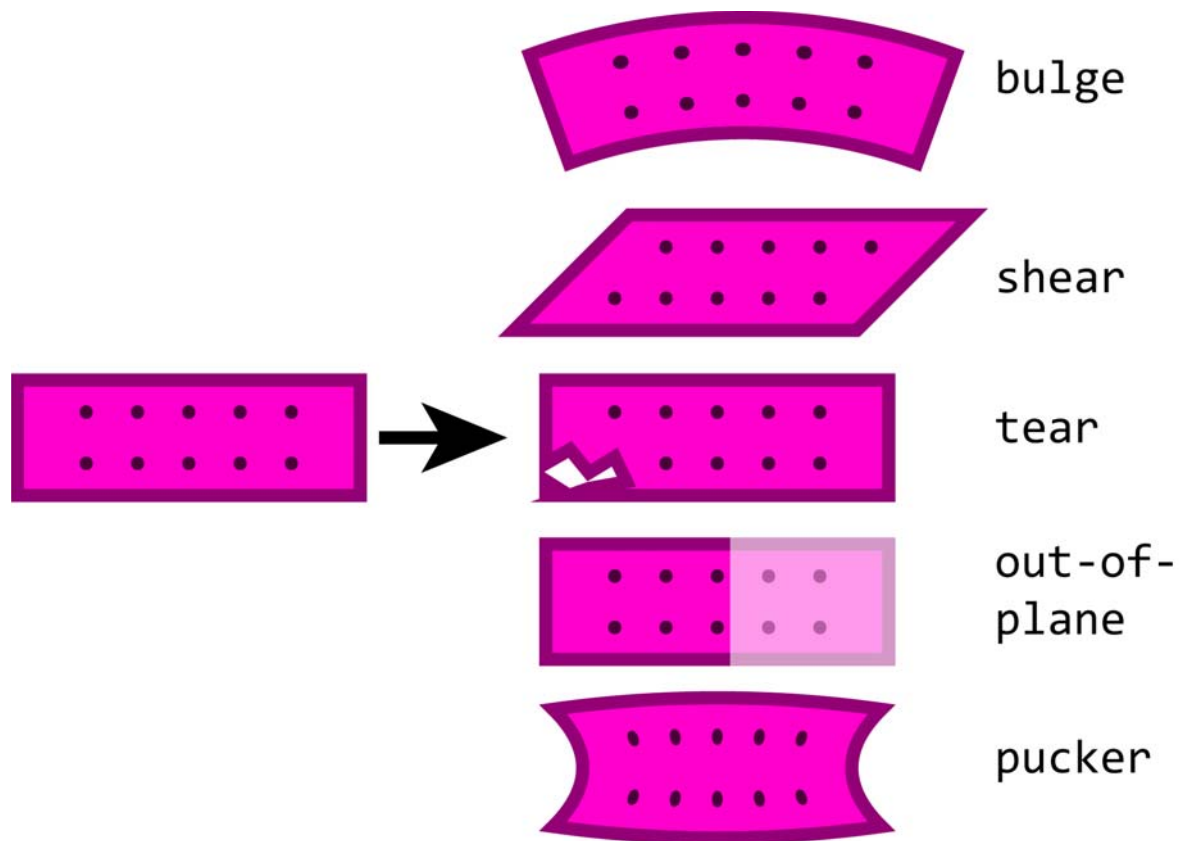


Figure 4-2. Bestiary of 3D transfer distortions. Various gel deformations can occur upon 3D transfer, mainly owing to imperfections in the manual manipulations required to remove the PDMS flow cell from the patterned glass surface.

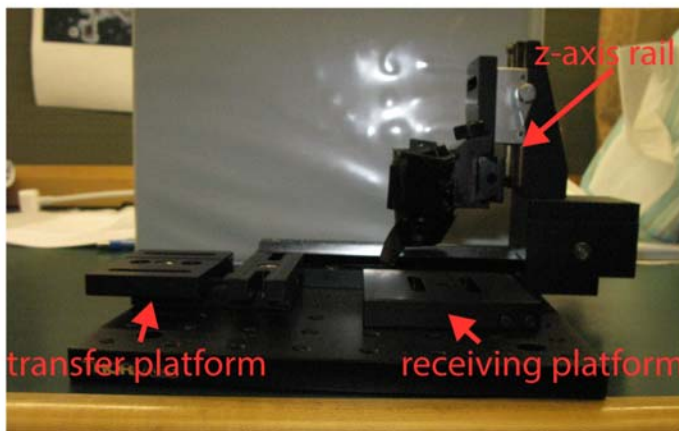
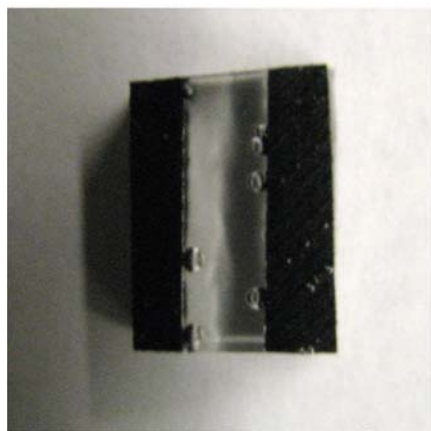
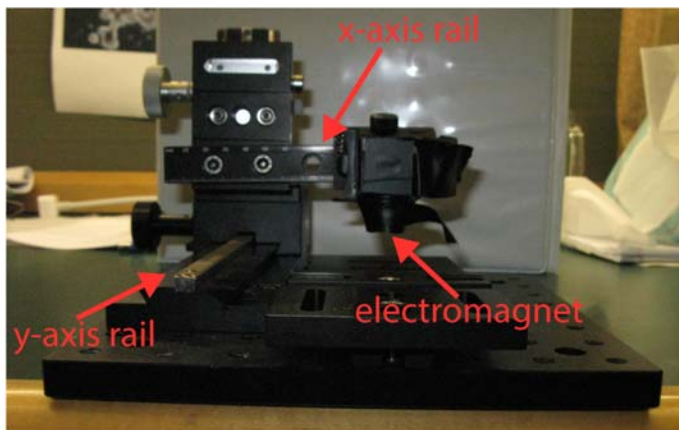
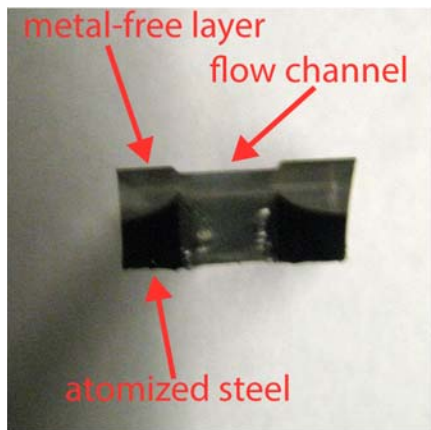


Figure 4-3. Components for magnetic lifting. Top left, an end-on view of a flow cell impregnated with atomized steel. Bottom left, a top-down view, showcasing the transparent flow channel. Top right, a view of a magnetic lifting apparatus. Bottom right, is a 90-degree rotation. Note the three rails permitting motion of the electromagnet relative to the transfer and receiving platforms.

4-2 Applications worth striving for.

When developing a technology platform, one can be overwhelmed by the number of possible applications that open up. This is especially relevant when developing a platform that enables questions to be asked, or things to be built, that were simply impossible previously. However, there is only so much time available, and one must carefully choose the best use of it. In this section, I outline what I believe are the most valuable projects to be pursued with CPA and attempt to justify my selections.

I assert that the single most valuable potential application of CPA is the synthesis of human microtissue arrays for use as a model system, especially with regards to drug discovery or testing genetic interventions. With regards to drug discovery, non-human model organisms are used to bypass the cost and ethical restrictions related to direct human testing. However, if human systems can be directly tested, then what use is there for the non-human models? Human microtissue arrays have the advantages of being cheaper than whole organisms and permit observations on thousands of identical microtissues. The prospect grows even more enticing when considering the possibility that human microtissue arrays could be synthesized using an individual's stem cells as the feedstock.

To reach a point where such human microtissue arrays are feasible, several goals must be met. First, and most trivially, arrays must be perfectly flat relative to their culture vessel, such that they are compatible with high-throughput imaging systems. Second, conditions to increase culture duration must be determined. In the field of tissue engineering, most observations are recorded within several days of synthesis. When determining if a drug is safe or efficacious, or in

some cases even determining if a microtissue is functional in the first place, it is necessary to grow cultures for much longer times. Months would be desirable. It is not obvious what is necessary to keep microtissues healthy for such a period. Pertinent questions would include what media to use, how frequently media should be changed, what accessory cells are required, how to avoid contamination, and whether standard gas mixtures like 5% carbon dioxide and 20% oxygen are sufficient for healthy microtissues for extended periods. Towards making these microtissue arrays, the third goal is determining what are the minimum requirements to synthesize adequately functional tissue. For our current studies in the mammary gland, we seek glandular tissue that is bilayered, lumenized, hormone-responsive, secretory, and contractile. The goals will change depending on the tissue of interest. But specific, measurable, achievable goals must be determined for these arrays to be successful.

I assert that the single most interesting tissue to synthesized with CPA will be neuronal circuits. Neural tissue is uniquely inaccessible to current techniques, and the knowledge to be gained from understanding it dwarfs any other tissue system. The nature of neurons is such that most of the information content of the system is stored in the connections between cells. Furthermore, there are numerous types of neurons, and the functionality of these neurons typically requires accessory cells such as oligodendrocytes and astrocytes. The cells are extremely delicate and tend to be scarce due to their non-proliferative nature. This combination of factors plays to all the strengths of CPA. By synthesizing minimal functional neuronal circuits, it may very well be possible to approach neuroscience from a reductionist perspective, something that the field has essentially abandoned due to its heretofore infeasibility.

5 REFERENCES

1. Debnath, J., Muthuswamy, S. K. & Brugge, J. S. Morphogenesis and oncogenesis of MCF-10A mammary epithelial acini grown in three-dimensional basement membrane cultures. *Methods* **30**, 256–268 (2003).
2. Paul, C. *et al.* Comparative histology of the adult electric organ among four species of the genus *Campylomormyrus* (Teleostei: Mormyridae). *J. Comp. Physiol. A* **201**, 357–374 (2015).
3. Asakura, T. *et al.* Some Observations on the Structure and Function of the Spinning Apparatus in the Silkworm *Bombyx mori*. *Biomacromolecules* **8**, 175–181 (2007).
4. Weiner, S., Traub, W. & Wagner, H. D. Lamellar Bone: Structure–Function Relations. *J. Struct. Biol.* **126**, 241–255 (1999).
5. Vogt, A. K., Wrobel, G., Meyer, W., Knoll, W. & Offenhäusser, A. Synaptic plasticity in micropatterned neuronal networks. *Biomaterials* **26**, 2549–2557 (2005).
6. Mendelsohn, A. D., Nyitray, C., Sena, M. & Desai, T. A. Size-controlled insulin-secreting cell clusters. *Acta Biomater.* **8**, 4278–4284 (2012).
7. Albrecht, D. R., Underhill, G. H., Wassermann, T. B., Sah, R. L. & Bhatia, S. N. Probing the role of multicellular organization in three-dimensional microenvironments. *Nat. Methods* **3**, 369–375 (2006).
8. Cerchiari, A. *et al.* Formation of Spatially and Geometrically Controlled Three-Dimensional Tissues in Soft Gels by Sacrificial Micromolding. *Tissue Eng. Part C Methods* (2014).
doi:10.1089/ten.tec.2014.0450

9. Nguyen-Ngoc, K.-V. *et al.* ECM microenvironment regulates collective migration and local dissemination in normal and malignant mammary epithelium. *Proc. Natl. Acad. Sci.* **109**, E2595–E2604 (2012).
10. Liu, J. S., Farlow, J. T., Paulson, A. K., Labarge, M. A. & Gartner, Z. J. Programmed Cell-to-Cell Variability in Ras Activity Triggers Emergent Behaviors during Mammary Epithelial Morphogenesis. *Cell Rep.* **2**, 1461–1470 (2012).
11. Pirlo, R. K., Wu, P., Liu, J. & Ringeisen, B. PLGA/hydrogel biopapers as a stackable substrate for printing HUVEC networks via BioLP™. *Biotechnol. Bioeng.* **109**, 262–273 (2012).
12. Hsiao, S. C. *et al.* Direct Cell Surface Modification with DNA for the Capture of Primary Cells and the Investigation of Myotube Formation on Defined Patterns. *Langmuir* **25**, 6985–6991 (2009).
13. Gartner, Z. J. & Bertozzi, C. R. Programmed assembly of 3-dimensional microtissues with defined cellular connectivity. *Proc. Natl. Acad. Sci.* **106**, 4606–4610 (2009).
14. Selden, N. S. *et al.* Chemically Programmed Cell Adhesion with Membrane-Anchored Oligonucleotides. *J. Am. Chem. Soc.* **134**, 765–768 (2012).
15. Bailey, R. C., Kwong, G. A., Radu, C. G., Witte, O. N. & Heath, J. R. DNA-Encoded Antibody Libraries: A Unified Platform for Multiplexed Cell Sorting and Detection of Genes and Proteins. *J. Am. Chem. Soc.* **129**, 1959–1967 (2007).
16. Teramura, Y., Chen, H., Kawamoto, T. & Iwata, H. Control of cell attachment through polyDNA hybridization. *Biomaterials* **31**, 2229–2235 (2010).
17. Application Note 203 - ‘Speed Printing’; or, printing in ‘No Laser Mode’ with the Nano eNabler System™. *BioForce Nanosciences* at

<<http://bioforcenano.com/resources/application-note-203-speed-printing-or-printing-in-no-laser-mode-with-the-nano-enabler-system/>>

18. Sweryda-Krawiec, B., Devaraj, H., Jacob, G. & Hickman, J. J. A New Interpretation of Serum Albumin Surface Passivation. *Langmuir* **20**, 2054–2056 (2004).
19. Vogt Jr., R. V., Phillips, D. L., Omar Henderson, L., Whitfield, W. & Spierto, F. W. Quantitative differences among various proteins as blocking agents for ELISA microtiter plates. *J. Immunol. Methods* **101**, 43–50 (1987).
20. Kannan, B., Castelino, K., Chen, F. F. & Majumdar, A. Lithographic techniques and surface chemistries for the fabrication of PEG-passivated protein microarrays. *Biosens. Bioelectron.* **21**, 1960–1967 (2006).
21. Xu, F. j. *et al.* Collagen-Coupled Poly(2-hydroxyethyl methacrylate)–Si(111) Hybrid Surfaces for Cell Immobilization. *Tissue Eng.* **11**, 1736–1748 (2005).
22. Massia, S. P. & Stark, J. Immobilized RGD peptides on surface-grafted dextran promote biospecific cell attachment. *J. Biomed. Mater. Res.* **56**, 390–399 (2001).
23. Luk, V. N., Mo, G. C. & Wheeler, A. R. Pluronic Additives: A Solution to Sticky Problems in Digital Microfluidics. *Langmuir* **24**, 6382–6389 (2008).
24. Arkles, B. Hydrophobicity, Hydrophilicity, and Silanes. (2006). at <<http://www.gelest.com/goods/pdf/Library/advances/HydrophobicityHydrophilicityandSilanes.pdf>>
25. Tripp, C. P. & Hair, M. L. Chemical attachment of chlorosilanes to silica: a two-step amine-promoted reaction. *J. Phys. Chem.* **97**, 5693–5698 (1993).


26. Kanan, S. M., Tze, W. T. Y. & Tripp, C. P. Method to Double the Surface Concentration and Control the Orientation of Adsorbed (3-Aminopropyl)dimethylethoxysilane on Silica Powders and Glass Slides. *Langmuir* **18**, 6623–6627 (2002).
27. Kinkel, J. N. & Unger, K. K. Role of solvent and base in the silanization reaction of silicas for reversed-phase high-performance liquid chromatography. *J. Chromatogr. A* **316**, 193–200 (1984).
28. Monserud, J. H. & Schwartz, D. K. Effects of Molecular Size and Surface Hydrophobicity on Oligonucleotide Interfacial Dynamics. *Biomacromolecules* **13**, 4002–4011 (2012).
29. Elder, R. M. & Jayaraman, A. Structure and thermodynamics of ssDNA oligomers near hydrophobic and hydrophilic surfaces. *Soft Matter* **9**, 11521–11533 (2013).
30. Lindahl, T. & Nyberg, B. Rate of depurination of native deoxyribonucleic acid. *Biochemistry (Mosc.)* **11**, 3610–3618 (1972).
31. Muller, W. Mammary Whole Mounts. at <http://tgmouse.compmed.ucdavis.edu/25table.HTM>
32. Roscoe B. Jackson Memorial Laboratory & Green, E. L. *Biology of the laboratory mouse*,. (Blakiston Division, McGraw-Hill, 1966).
33. Dawson, P. J., Wolman, S. R., Tait, L., Heppner, G. H. & Miller, F. R. MCF10AT: a model for the evolution of cancer from proliferative breast disease. *Am. J. Pathol.* **148**, 313–319 (1996).

Publishing Agreement

It is the policy of the University to encourage the distribution of all theses, dissertations, and manuscripts. Copies of all UCSF theses, dissertations, and manuscripts will be routed to the library via the Graduate Division. The library will make all theses, dissertations, and manuscripts accessible to the public and will preserve these to the best of their abilities, in perpetuity.

Please sign the following statement:

I hereby grant permission to the Graduate Division of the University of California, San Francisco to release copies of my thesis, dissertation, or manuscript to the Campus Library to provide access and preservation, in whole or in part, in perpetuity.



Author Signature

3/15/15

Date